projection neurons. Activity patterns of other interneurons during task performance remain to be studied. The striatum is classified into μ-opiate receptor-rich patch compartment (or striosome) and matrix compartment (Graybiel, 1990), but the relationship between somatotopy and patch-matrix organization is unclear.

Other motor cortices also project to the striatum (**Figure 3B**; Takada et al., 1998a,b, 2001; Inase et al., 1999; Tachibana et al., 2004). The highest motor cortices, such as pre-SMA, PMdr, and CMAr, project to the anterior part of the striatum, especially to the bridge region connecting the caudate nucleus and putamen. The forelimb regions of the PMdc and PMvc project to two independent regions in the SMA territory of the putamen. On the other hand, the CMAc, which shows activity similar to that of the MI, projects to the MI territory. Projections from the primary somatosensory cortex also project to the MI territory (Flaherty and Graybiel, 1993). The projection patterns seem to obey the following rules: The motor cortices whose functions are distinct project to the different regions of the striatum, whereas the motor cortices whose functions are similar project to the common striatal regions in a convergent manner. The prefrontal cortex projects to the rostral part of the putamen anterior to the anterior commissure and the head of the caudate nucleus (prefrontal territory of the striatum), and the limbic cortex projects to the ventral striatum (limbic territory; Selemon and Goldman-Rakic, 1985; Haber et al., 1990; Parent, 1990). Eye movement-related neurons are located in the central part of the caudate nucleus (oculomotor territory; Hikosaka et al., 1989).

SUBTHALAMIC NUCLEUS (STN)

The STN, another input station of the basal ganglia, receives cortical inputs from the frontal lobe. The dorsal part of the STN is the motor territory and shows somatotopic organization (**Figure 4A**; Monakow et al., 1978; Nambu et al., 1996). The MI projects to the lateral part (MI territory), and the SMA projects to the medial part (SMA territory). The orofacial, forelimb, and hindlimb regions of the MI project to the lateral to medial parts of the lateral STN, while those of the SMA project to the medial to lateral parts of the medial STN. Therefore, two sets of somatotopic representations, which are mirror images of each other, are represented in the lateral and medial parts of the STN. The MI also partly projects to the somatotopically corresponding body parts in the SMA territory, and the SMA partly projects to the MI territory, vice versa. Thus, inputs from the MI and SMA partly converge in the STN. The forelimb regions of the PMdc and PMvc also project to the forelimb region of the SMA territory (**Figure 4B**; Nambu et al., 1997). The somatotopy of the STN reflects not only input organization, but also output organization, because similar somatotopy is observed after transneuronal retrograde labeling of rabies virus by its injection into the MI (Miyachi et al., 2006).

The somatotopy of the STN has also been confirmed by electrophysiological methods. Cortical stimulation of the MI and SMA induces a short latency excitation and a subsequent long latency excitation (Nambu et al., 2000), which are mediated by the cortico-STN (hyperdirect) and cortico-striato-GPe-STN (indirect) pathways, respectively. By observing cortically evoked responses, similar somatotopy can be drawn, with some neurons receiving convergent inputs from the MI and SMA. STN neurons in the MI territory change their activity (mostly excitation) in relation to active or passive movements of the corresponding body parts on the contralateral side (DeLong et al., 1985; Wichmann et al., 1994). STN neurons in the SMA territory may also show task-related activity. Microstimulation in the MI and SMA territories does not evoke movements, while that in the most lateral part of the STN often evokes movements probably because of the current spread to the internal capsule (Wichmann et al., 1994).

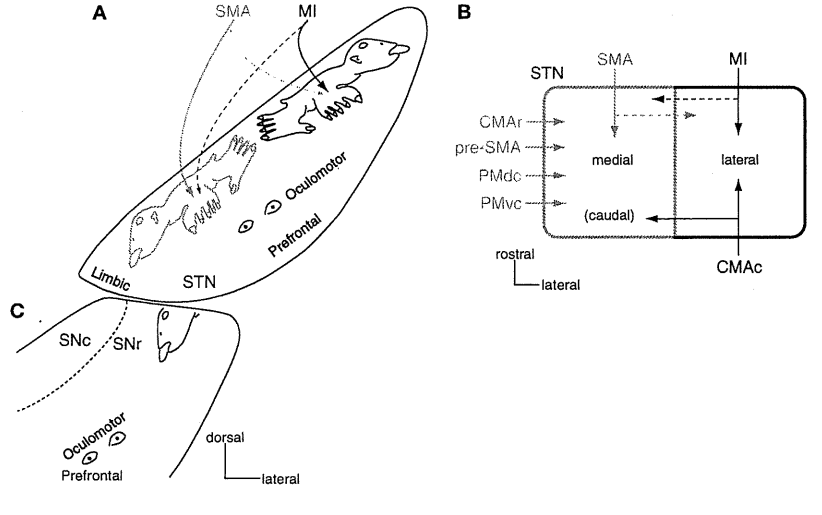

FIGURE 4 | Somatotopy of the subthalamic nucleus (STN) and substantia nigra (SN). (A) Somatotopy of the STN is shown in a frontal section. In the dorsal part of the STN, the lateral part receives somatotopic inputs from the MI, and the medial part from the SMA. The MI also projects partly to the medial part, and the SMA to the lateral part. Ventral to the motor territory, there exist the oculomotor and prefrontal territories. The most medial part is occupied by the limbic territory. Modified from Nambu et al. (2002b). **(B)** Input from motor cortices to the STN is schematically shown in a horizontal section. Modified from Takada et al. (2001). **(C)** Somatotopy of the SNr is shown in a frontal section. The orofacial region of the SNr is a continuation of that of the GPi (see **Figure 5**). Ventral to the motor territory, there exist the oculomotor and prefrontal territories.

Concerning other motor cortical inputs, the CMAc projects to the MI territory of the STN, and the pre-SMA and CMAr project to the SMA territory (**Figure 4B**; Inase et al., 1999; Takada et al., 2001). Thus, more convergence may occur in the cortico-STN projections than in the cortico-striatal projections (compare **Figure 4B** with **Figure 3B**), suggesting that the hyperdirect pathway assembles information from more wide areas of the motor cortices than the direct and indirect pathways do. Ventral to the motor territory in the STN, there exist the oculomotor territory (Matsumura et al., 1992) and the prefrontal territory (Monakow et al., 1978; Parent, 1990; **Figure 4A**). The most ventromedial part of the STN is occupied by the limbic territory (Parent, 1990).

EXTERNAL AND INTERNAL SEGMENTS OF THE GLOBUS PALLIDUS (GPe AND GPi)

The motor territory of the striatum (i.e., the caudal aspect of the putamen) projects to the ventral two-thirds of the caudal GPe and GPi, and thus, these areas are the motor territories of the globus pallidus (Smith and Parent, 1986; Parent, 1990) that show somatotopic organization (**Figure 5**). In GPe/GPi neurons, cortical stimulation evokes a triphasic response composed of early excitation, inhibition, and late excitation, which are mediated by the cortico-STN-GPe/GPi (cortico-STN-GPi: hyperdirect), cortico-striato-GPe/GPi (cortico-striato-GPi: direct), and cortico-striato-GPe-STN-GPe/GPi (cortico-striato-GPe-STN-GPi: indirect) pathways, respectively (Nambu et al., 2000; Kita et al., 2004; Tachibana et al., 2008). The somatotopy in the GPe/GPi can be drawn by observing responses evoked by the stimulation of the MI and SMA. Neurons responding to the orofacial, forelimb, and hindlimb regions of the MI are located along the ventral-to-dorsal axis in the GPe and GPi (MI territory, **Figure 5**; Yoshida et al., 1993). Neurons responding to the corresponding regions of the SMA are also located along the ventral-to-dorsal axis, but in more rostral and dorsal parts of the GPe/GPi (SMA territory). Stimulation of the PM also evokes responses in the SMA territory. GPe/GPi neurons rarely respond to cortical stimulation of multiple body parts, and thus, the orofacial, forelimb, and hindlimb regions of GPe/GPi are clearly and distinctly identified. On the other hand, many neurons respond to the stimulation of both the MI and SMA, and the somatotopic representation in the MI territory and that in the SMA territory are partly fused in the rostro-caudal central zone. Most GPe/GPi neurons show triphasic responses evoked by cortical stimulation, suggesting that the hyperdirect, direct, and indirect pathways originating from a certain body region in the cortex converge at a single GPe/GPi neuronal level.

The above-mentioned somatotopy is also supported by anatomical studies. The injection of anterograde tracers into the MI, SMA, and convergent territories in the putamen revealed the terminals in the GPe/GPi (Kaneda et al., 2002). Terminals from the SMA territory of the putamen are located more anterior and dorsal to those from the MI territory. The convergent territory of the putamen projects to the area in-between, and these three projection territories do not overlap. Transsynaptic anterograde and retrograde labeling studies by injecting herpes simplex virus into the MI reported similar results (Hoover and Strick, 1993, 1999; Strick et al., 1995; Akkal et al., 2007), although there is some discrepancy, such as that the PMv territory of the GPe/GPi is located ventrally to the MI territory. Dendritic fields of GPe/GPi neurons extend widely in the direction perpendicular to the striato-pallidal fibers, and this is considered to be the basis for information convergence (Percheron et al., 1984; Yelnik et al., 1984). However, somatotopic organization through the striato-pallidal projections is well preserved as described above.

Neurons in the MI and SMA territories of the GPe/GPi change their activity in relation to active and passive movements of the corresponding body parts on the contralateral side (DeLong, 1971; Georgopoulos et al., 1983; DeLong et al., 1985; Hamada et al., 1990). However, response patterns are different between these territories. Neurons in the MI territory show movement-related activity, while those in the SMA territory show delay-related activity (Nambu et al., 1990). On the other hand, response patterns in the GPe and GPi neurons during task performance are very similar. Microstimulation in the GPe/GPi does not induce any movements.

The prefrontal territory of the striatum projects to the rostral GPe and dorsal one-third of the caudal GPe/GPi, and thus, these areas are the prefrontal territory (Smith and Parent, 1986; Parent, 1990). Ventral striatum projects to the VP, the most rostral part of the GPe and the most medial part of the GPi, and thus, these areas correspond to the limbic territory (Haber et al., 1990; Parent, 1990).

SUBSTANTIA NIGRA (SN)

The SNr and GPi are the output nuclei of the basal ganglia and considered to be a continuum, which is divided into the SNr and GPi by the internal capsule. The motor territory of the striatum projects to the dorsal one-third of the SNr, and thus, this area is considered to be the motor territory of the SNr (**Figure 4C**; Smith and Parent, 1986; Parent, 1990). Neurons in the dorsolateral part

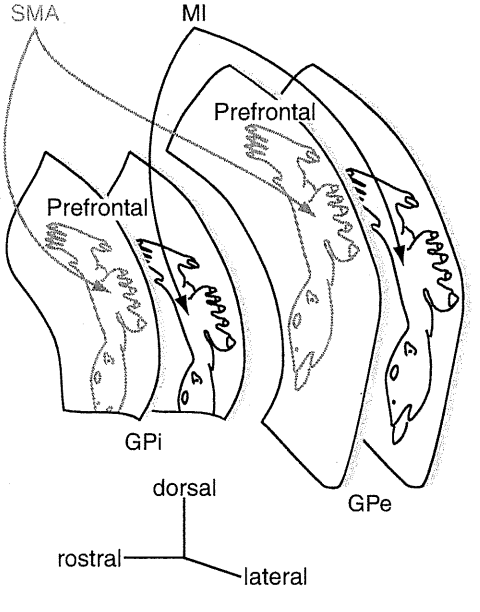

FIGURE 5 | Somatotopy of the external and internal segments of the globus pallidus (GPe and GPi). The GPe and GPi have their own somatotopic representations. The somatotopy in the SMA territory is located rostrodorsally to that in the MI territory. Two territories overlap partly in the rostro-caudal zone. Dorsal one-third of the GPe/GPi is occupied by the prefrontal territory.

of this area respond to the stimulation of the MI, especially to that of the orofacial region, and change their activity in relation to active or passive movements of the orofacial region (DeLong et al., 1983; Kitano et al., 1998). The orofacial region of the SNr is considered to be a continuation of the orofacial region of the GPi (see **Figures 4C and 5**). SNr neurons in the part ventral to the orofacial region receive inputs from the SMA territories of the putamen, and change their activity during task performance. However, the somatotopy is not clearly organized, and their activity is not so distinct compared to that of GPi neurons (Wichmann and Kliem, 2004). The prefrontal territory of the striatum projects to the rostromedial two-thirds of the SNr (Smith and Parent, 1986) that also include the oculomotor territory (Hikosaka and Wurtz, 1983; **Figure 4C**). The limbic territory of the striatum projects to the most medial part of the SNr (Haber et al., 1990).

The SNc is composed of dopaminergic neurons, and projects to the striatum and other basal ganglia nuclei. Dopaminergic projections from the SNc to the striatum display weak topography, and the terminal fields of a single dopaminergic neuron are large (Parent et al., 1983; Parent, 1990; Matsuda et al., 2009). SNc neurons do not respond to active or passive body part movements, but respond to novel sensory stimuli and/or rewards (DeLong et al., 1983; Schultz and Romo, 1990). Recent studies suggest that SNc neurons code the difference between the expected reward and the real reward (a temporal difference error in reinforcement learning). These observations suggest that the SNc has no clear somatotopy.

THALAMUS

The motor thalamus is a target structure of the basal ganglia, and also shows somatotopy (**Figure 6**). Subnuclei located in the rostral part of the motor thalamus receive inputs from the basal ganglia. The oral part of the ventrolateral nucleus (VLo) and the principal part of the ventroanterior nucleus (VApc) receive inputs from the GPi. The medial part of the ventrolateral nucleus (VLm) and the magnocellular part of the ventroanterior nucleus (VAmc) receive inputs from the SNr. On the other hand, subnuclei located in the caudal part, such as the oral part of the ventroposterolateral nucleus (VPLo), the caudal part of the ventrolateral nucleus (VLc) and area X, receive cerebellar inputs (Jones, 2007). Thus, projections from the SNr, GPi and cerebellar nuclei terminate in the rostral to caudal parts of the motor thalamus, and the overlap of their terminals is minimal. The VApc, VLo, VPLo, and VLc project to the motor cortices, and thus, most of the motor cortices receive inputs from both the basal ganglia and the cerebellum through the motor thalamus (Jones, 2007). The MI receives basal ganglia inputs through the VLo, and cerebellar inputs through the VPLo (Holsapple et al., 1991).

The VLo and VPLo display clear somatotopic organization (**Figure 6**). The orofacial, forelimb, and hindlimb regions are represented in the medial to lateral parts (Asanuma et al., 1983; Vitek et al., 1994). VLo neurons change their activity in relation to active movements of the corresponding body parts (Anderson and Turner, 1991; Nambu et al., 1991; Vitek et al., 1994). However, sensory inputs are not clearly identified, and the microstimulation in the VLo does not induce any movements (Buford et al., 1996; Vitek et al., 1996). On the other hand, VPLo neurons respond clearly to active and passive movements of discrete body parts (one to several joints) on the contralateral side. Microstimulation in the VPLo induces movements in the corresponding body parts, contralateral to the stimulation side. The somatotopy can also be confirmed by the anatomical study of the thalamo-cortical projections (Asanuma et al., 1983; Holsapple et al., 1991). Therefore, the thalamus has at least two sets of somatotopic representations: one in the GPi-receiving region (VLo) and the other in the cerebellar-receiving region (VPLo).

FUNCTIONAL SIGNIFICANCE OF THE SOMATOTOPY

Each nucleus of the basal ganglia shows clear somatotopic organization, and information originating from cortical regions representing different body parts rarely converges in the cortico-basal ganglia circuitry. These observations suggest that information related to different body parts, such as forelimb and hindlimb, is processed independently through the cortico-basal ganglia loop. On the other hand, information from different but related cortical areas, such as the forelimb regions of the MI and SMA, is processed in both convergent and non-convergent manners. However, the functional roles of such convergence remain to be elucidated.

SOMATOTOPY AND MOVEMENT DISORDERS

The pathophysiology of movement disorders can be explained by the changes of the firing rates and patterns in the basal ganglia, especially in the GPe, GPi, and STN. In addition, changes in the somatotopy have been reported in movement disorders. In a normal state, GPe and GPi neurons respond specifically to the movement of one direction of a single joint on the contralateral side. On the other hand, GPe/GPi neurons in a Parkinsonian state respond to multiple movements of multiple joints, sometimes of the upper and lower limbs and of both sides (Filion et al., 1988). Loss of functional segregation was also reported in the GPi-receiving thalamus (Pessiglione et al., 2005). Dopamine is considered to contribute to

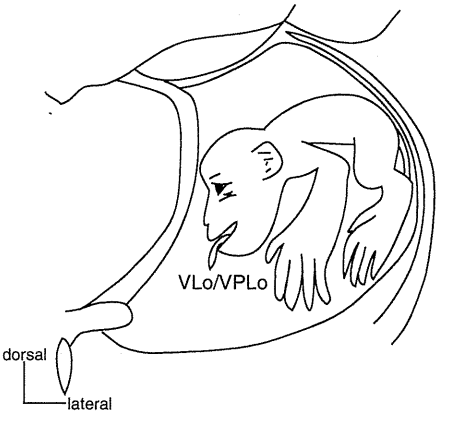

FIGURE 6 | Somatotopy of the thalamus. Somatotopy of the thalamus is shown in a frontal section. Both the oral part of the ventrolateral nucleus of the thalamus (VLo) receiving pallidal projections and the oral part of the ventroposterolateral nucleus of the thalamus (VPLo) receiving cerebellar projections have their own somatotopic representations. Their somatotopic representations are continuous rostrocaudally. Modified from Asanuma et al. (1983).

isolate information related to movements of specific body parts. Loss of dopamine may induce a crosstalk of information related to different body parts (Bergman et al., 1998).

In dystonia, somatotopy of the basal ganglia is also disorganized (Vitek et al., 1999; Chiken et al., 2008). GPe/GPi neurons respond to stimulation of multiple body parts, and they are intermingled. Dystonic patients show a phenomenon known as "motor overflow." Such a phenomenon may be explained by disorganization of the somatotopy. When patients try to move one body part, for example, a hand, not only the hand region, but also other regions, such as the neck region, of the GPi could be inhibited by somatotopic disorganization. This may lead to unintended movements of other body parts, such as the neck, that accompany intended movements of a hand.

Hemiballism is caused by lesions in the STN, such as a hemorrhage or infarction. Hemiballism in the lower limb is common, while that in the orofacial regions is rare (Carpenter et al., 1950; Hamada and DeLong, 1992). Hemiballism in the upper limb is associated with that in the lower limb. These characteristics can be explained by the mirror image organization of the somatotopy in the STN (**Figure 4A**; Nambu et al., 1996). It is supposed that the inactivation of both the MI and SMA territories of the corresponding body parts is necessary to produce hemiballism. Small lesions in the central STN affect both lower limb regions of the MI and SMA territories, and thus cause hemiballism in the lower limb. Large lesions affecting both upper limb regions of the MI and SMA territories also affect both lower limb regions, and thus hemiballism in the upper limb is accompanied by that in the lower limb. Lesions affecting both orofacial regions of the MI and SMA territories should be rare because they are remotely located.

Abnormal firing rates and patterns in the motor territory of the basal ganglia cause motor symptoms of the movement disorders. The target of stereotaxic surgery, including deep brain stimulation (DBS), for treatment of movement disorders aimed at the motor territory of the basal ganglia, such as the GPi and STN. The somatotopy gives us useful indices to identify the targets during stereotaxic surgery (Kaplitt et al., 2003). STN-DBS sometimes induces side effects of mood changes. This may be explained by the current spread from the motor territory to the limbic and prefrontal territories of the STN because of the small size of the STN. On the other hand, GP-DBS does not induce psychological side effects, probably because the motor territory is remotely located from the limbic and prefrontal territories in the GPi.

CONCLUSION

In this article, I have described that each nucleus of the basal ganglia shows clear somatotopic organization, and that information related to different body parts is processed independently through the cortico-basal ganglia loop. I would like to point out the following unsolved questions: In the topographic projections from one nucleus to another nucleus, what kind of information is added? What kind of information is originated? How do converging inputs from multiple motor cortices contribute to the execution of voluntary movements? How is the somatotopy in each nucleus of the basal ganglia organized during development? These are important questions closely related to the functions of the basal ganglia. The somatotopic perspective way of view will be a good clue and guide for further understanding of the basal ganglia.

ACKNOWLEDGMENTS

Studies in the author's laboratory were supported by Grants-in-Aid for Scientific Research from the Ministry of Education, Culture, Sports, Science, and Technology of Japan. The author is grateful to the current and former collaborators.

REFERENCES

Akkal, D., Dum, R. P., and Strick, P. L. (2007). Supplementary motor area and presupplementary motor area: targets of basal ganglia and cerebellar output. *J. Neurosci.* 27, 10659–10673.

Alexander, G. E., and Crutcher, M. D. (1990a). Functional architecture of basal ganglia circuits: neural substrates of parallel processing. *Trends Neurosci.* 13, 266–271.

Alexander, G. E., and Crutcher, M. D. (1990b). Preparation for movement: neural representations of intended direction in three motor areas of the monkey. *J. Neurophysiol.* 64, 133–150.

Alexander, G. E., and DeLong, M. R. (1985). Microstimulation of the primate neostriatum. II. Somatotopic organization of striatal microexcitable zones and their relation to neuronal response properties. *J. Neurophysiol.* 53, 1417–1430.

Alexander, G. E., DeLong, M. R., and Strick, P. L. (1986). Parallel organization of functionally segregated circuits linking basal ganglia and cortex. *Annu. Rev. Neurosci.* 9, 357–381.

Anderson, M. E., and Turner, R. S. (1991). Activity of neurons in cerebellar-receiving and pallidal-receiving areas of the thalamus of the behaving monkey. *J. Neurophysiol.* 66, 879–893.

Aosaki, T., Kimura, M., and Graybiel, A. M. (1995). Temporal and spatial characteristics of tonically active neurons of the primate's striatum. *J. Neurophysiol.* 73, 1234–1252.

Asanuma, C., Thach, W. R., and Jones, E. G. (1983). Anatomical evidence for segregated focal groupings of efferent cells and their terminal ramifications in the cerebellothalamic pathway of the monkey. *Brain Res.* 286, 267–297.

Bergman, H., Feingold, A., Nini, A., Raz, A., Slovin, H., Abeles, M., and Vaadia, E. (1998). Physiological aspects of information processing in the basal ganglia of normal and Parkinsonian primates. *Trends Neurosci.* 21, 32–38.

Buford, J. A., Inase, M., and Anderson, M. E. (1996). Contrasting locations of pallidal-receiving neurons and microexcitable zones in primate thalamus. *J. Neurophysiol.* 75, 1105–1116.

Carpenter, M. B., Whittier, J. R., and Mettler, F. A. (1950). Analysis of choreoid hyperkinesia in the Rhesus monkey; surgical and pharmacological analysis of hyperkinesia resulting from lesions in the subthalamic nucleus of Luys. *J. Comp. Neurol.* 92, 293–331.

Chiken, S., Shashidharan, P., and Nambu, A. (2008). Cortically evoked long-lasting inhibition of pallidal neurons in a transgenic mouse model of dystonia. *J. Neurosci.* 28, 13967–13977.

DeLong, M. R. (1971). Activity of pallidal neurons during movement. *J. Neurophysiol.* 34, 414–427.

DeLong, M. R., Crutcher, M. D., and Georgopoulos, A. P. (1983). Relations between movement and single cell discharge in the substantia nigra of the behaving monkey. *J. Neurosci.* 3, 1599–1606.

DeLong, M. R., Crutcher, M. D., and Georgopoulos, A. P. (1985). Primate globus pallidus and subthalamic nucleus: functional organization. *J. Neurophysiol.* 53, 530–543.

Filion, M., Tremblay, L., and Bedard, P. J. (1988). Abnormal influences of passive limb movement on the activity of globus pallidus neurons in Parkinsonian monkeys. *Brain Res.* 444, 165–176.

Flaherty, A. W., and Graybiel, A. M. (1993). Two input systems for body representations in the primate striatal matrix: experimental evidence in the squirrel monkey. *J. Neurosci.* 13, 1120–1137.

Gage, G. J., Stoetzner, C. R., Wiltschko, A. B., and Berke, J. D. (2010). Selective activation of striatal fast-spiking interneurons during choice execution. *Neuron* 67, 466–479.

Georgopoulos, A. P., DeLong, M. R., and Crutcher, M. D. (1983). Relations between parameters of step-tracking movements and single cell discharge in the globus pallidus and subthalamic nucleus of the behaving monkey. *J. Neurosci.* 3, 1586–1598.

Graybiel, A. M. (1990). Neurotransmitters and neuromodulators in the basal ganglia. *Trends Neurosci.* 13, 244–254.

Haber, S. N., Kim, K. S., Mailly, P., and Calzavara, R. (2006). Reward-related cortical inputs define a large striatal region in primates that interface with

associative cortical connections, providing a substrate for incentive-based learning. *J. Neurosci.* 26, 8368–8376.

Haber, S. N., Lynd, E., Klein, C., and Groenewegen, H. J. (1990). Topographic organization of the ventral striatal efferent projections in the rhesus monkey: an anterograde tracing study. *J. Comp. Neurol.* 293, 282–298.

Hamada, I., and DeLong, M. R. (1992). Excitotoxic acid lesions of the primate subthalamic nucleus result in transient dyskinesias of the contralateral limbs. *J. Neurophysiol.* 68, 1850–1858.

Hamada, I., Delong, M. R., and Mano, N. (1990). Activity of identified wrist-related pallidal neurons during step and ramp wrist movements in the monkey. *J. Neurophysiol.* 64, 1892–1906.

Hikosaka, O., Sakamoto, M., and Usui, S. (1989). Functional properties of monkey caudate neurons. I. Activities related to saccadic eye movements. *J. Neurophysiol.* 61, 780–798.

Hikosaka, O., and Wurtz, R. H. (1983). Visual and oculomotor functions of monkey substantia nigra pars reticulata. I. Relation of visual and auditory responses to saccades. *J. Neurophysiol.* 49, 1230–1253.

Holsapple, J. W., Preston, J. B., and Strick, P. L. (1991). The origin of thalamic inputs to the "hand" representation in the primary motor cortex. *J. Neurosci.* 11, 2644–2654.

Hoover, J. E., and Strick, P. L. (1993). Multiple output channels in the basal ganglia. *Science* 259, 819–821.

Hoover, J. E., and Strick, P. L. (1999). The organization of cerebellar and basal ganglia outputs to primary motor cortex as revealed by retrograde transneuronal transport of herpes simplex virus type 1. *J. Neurosci.* 19, 1446–1463.

Inase, M., Tokuno, H., Nambu, A., Akazawa, T., and Takada, M. (1999). Corticostriatal and corticosubthalamic input zones from the presupplementary motor area in the macaque monkey: comparison with the input zones from the supplementary motor area. *Brain Res.* 833, 191–201.

Jones, E. G. (2007). *The Thalamus*. New York: Cambridge University Press.

Kaneda, K., Nambu, A., Tokuno, H., and Takada, M. (2002). Differential processing patterns of motor information via striatopallidal and striatonigral projections. *J. Neurophysiol.* 88, 1420–1432.

Kaplitt, M. G., Hutchinson, W. D., and Lozano, A. M. (2003). "Target localization in movement disorders surgery," in *Surgical Treatment of Parkinson's Disease and Other Movement Disorders*, eds D. Tarsy, J. L. Vitek, and A. M. Lozano (Totowa: Humana Press), 87–98.

Kita, H., Nambu, A., Kaneda, K., Tachibana, Y., and Takada, M. (2004). Role of ionotropic glutamatergic and GABAergic inputs on the firing activity of neurons in the external pallidum in awake monkeys. *J. Neurophysiol.* 92, 3069–3084.

Kitano, H., Tanibuchi, I., and Jinnai, K. (1998). The distribution of neurons in the substantia nigra pars reticulata with input from the motor, premotor and prefrontal areas of the cerebral cortex in monkeys. *Brain Res.* 784, 228–238.

Künzle, H. (1975). Bilateral projections from precentral motor cortex to the putamen and other parts of the basal ganglia. An autoradiographic study in *Macaca fascicularis*. *Brain Res.* 88, 195–209.

Matsuda, W., Furuta, T., Nakamura, K. C., Hioki, H., Fujiyama, F., Arai, R., and Kaneko, T. (2009). Single nigrostriatal dopaminergic neurons form widely spread and highly dense axonal arborizations in the neostriatum. *J. Neurosci.* 29, 444–453.

Matsumura, M., Kojima, J., Gardiner, T. W., and Hikosaka, O. (1992). Visual and oculomotor functions of monkey subthalamic nucleus. *J. Neurophysiol.* 67, 1615–1632.

McFarland, N. R., and Haber, S. N. (2000). Convergent inputs from thalamic motor nuclei and frontal cortical areas to the dorsal striatum in the primate. *J. Neurosci.* 20, 3798–3813.

Miyachi, S., Lu, X., Imanishi, M., Sawada, K., Nambu, A., and Takada, M. (2006). Somatotopically arranged inputs from putamen and subthalamic nucleus to primary motor cortex. *Neurosci. Res.* 56, 300–308.

Monakow, K. H., Akert, K., and Künzle, H. (1978). Projections of the precentral motor cortex and other cortical areas of the frontal lobe to the subthalamic nucleus in the monkey. *Exp. Brain Res.* 33, 395–403.

Nakano, K., Hasegawa, Y., Tokushige, A., Nakagawa, S., Kayahara, T., and Mizuno, N. (1990). Topographical projections from the thalamus, subthalamic nucleus and pedunculopontine tegmental nucleus to the striatum in the Japanese monkey, *Macaca fuscata*. *Brain Res.* 537, 54–68.

Nambu, A., Kaneda, K., Tokuno, H., and Takada, M. (2002a). Organization of corticostriatal motor inputs in monkey putamen. *J. Neurophysiol.* 88, 1830–1842.

Nambu, A., Tokuno, H., and Takada, M. (2002b). Functional significance of the cortico-subthalamo-pallidal 'hyperdirect' pathway. *Neurosci. Res.* 43, 111–117.

Nambu, A., Takada, M., Inase, M., and Tokuno, H. (1996). Dual somatotopical representations in the primate subthalamic nucleus: evidence for ordered but reversed body-map transformations from the primary motor cortex and the supplementary motor area. *J. Neurosci.* 16, 2671–2683.

Nambu, A., Tokuno, H., Hamada, I., Kita, H., Imanishi, M., Akazawa, T., Ikeuchi, Y., and Hasegawa, N. (2000). Excitatory cortical inputs to pallidal neurons via the subthalamic nucleus in the monkey. *J. Neurophysiol.* 84, 289–300.

Nambu, A., Tokuno, H., Inase, M., and Takada, M. (1997). Corticosubthalamic input zones from forelimb representations of the dorsal and ventral divisions of the premotor cortex in the macaque monkey: comparison with the input zones from the primary motor cortex and the supplementary motor area. *Neurosci. Lett.* 239, 13–16.

Nambu, A., Yoshida, S., and Jinnai, K. (1990). Discharge patterns of pallidal neurons with input from various cortical areas during movement in the monkey. *Brain Res.* 519, 183–191.

Nambu, A., Yoshida, S., and Jinnai, K. (1991). Movement-related activity of thalamic neurons with input from the globus pallidus and projection to the motor cortex in the monkey. *Exp. Brain Res.* 84, 279–284.

Parent, A. (1990). Extrinsic connections of the basal ganglia. *Trends Neurosci.* 13, 254–258.

Parent, A., and Hazrati, L. N. (1995). Functional anatomy of the basal ganglia. I. The cortico-basal ganglia-thalamo-cortical loop. *Brain Res. Rev.* 20, 91–127.

Parent, A., Mackey, A., and De Bellefeuille, L. (1983). The subcortical afferents to caudate nucleus and putamen in primate: a fluorescence retrograde double labeling study. *Neuroscience* 10, 1137–1150.

Percheron, G., and Filion, M. (1991). Parallel processing in the basal ganglia: up to a point. *Trends Neurosci.* 14, 55–59.

Percheron, G., Francois, C., Yelnik, J., Fenelon, G., and Talbi, B. (1994). "The basal ganglia related system of primates: Definition, description and information analysis," in *The Basal Ganglia IV: New Ideas and Data on Structure and Function*, eds G. Percheron, J. S. McKenzie, and J. Feger (New York: Plenum Press), 3–20.

Percheron, G., Yelnik, J., and Francois, C. (1984). A Golgi analysis of the primate globus pallidus. III. Spatial organization of the striato-pallidal complex. *J. Comp. Neurol.* 227, 214–227.

Pessiglione, M., Guehl, D., Rolland, A. S., Francois, C., Hirsch, E. C., Feger, J., and Tremblay, L. (2005). Thalamic neuronal activity in dopamine-depleted primates: evidence for a loss of functional segregation within basal ganglia circuits. *J. Neurosci.* 25, 1523–1531.

Picard, N., and Strick, P. L. (2001). Imaging the premotor areas. *Curr. Opin. Neurobiol.* 11, 663–672.

Sadikot, A. F., Parent, A., Smith, Y., and Bolam, J. P. (1992). Efferent connections of the centromedian and parafascicular thalamic nuclei in the squirrel monkey: a light and electron microscopic study of the thalamostriatal projection in relation to striatal heterogeneity. *J. Comp. Neurol.* 320, 228–242.

Schultz, W., and Romo, R. (1990). Dopamine neurons of the monkey midbrain: contingencies of responses to stimuli eliciting immediate behavioral reactions. *J. Neurophysiol.* 63, 607–624.

Selemon, L. D., and Goldman-Rakic, P. S. (1985). Longitudinal topography and interdigitation of corticostriatal projections in the rhesus monkey. *J. Neurosci.* 5, 776–794.

Smith, Y., and Parent, A. (1986). Differential connections of caudate nucleus and putamen in the squirrel monkey (*Saimiri sciureus*). *Neuroscience* 18, 347–371.

Strick, P. L., Dum, R. P., and Picard, N. (1995). "Macro-organization of the circuits connecting the basal ganglia with the cortical motor areas," in *Models of Information Processing in the Basal Ganglia*, eds J. C. Houck, J. L. Davis, and D. G. Beiser (Cambridge: MIT Press), 117–130.

Tachibana, Y., Kita, H., Chiken, S., Takada, M., and Nambu, A. (2008). Motor cortical control of internal pallidal activity through glutamatergic and GABAergic inputs in awake monkeys. *Eur. J. Neurosci.* 27, 238–253.

Tachibana, Y., Nambu, A., Hatanaka, N., Miyachi, S., and Takada, M. (2004). Input-output organization of the rostral part of the dorsal premotor cortex, with special reference to its corticostriatal projection. *Neurosci. Res.* 48, 45–57.

Takada, M., Nambu, A., Hatanaka, N., Tachibana, Y., Miyachi, S., Taira, M., and Inase, M. (2004). Organization of prefrontal outflow toward frontal motor-related areas in macaque monkeys. *Eur. J. Neurosci.* 19, 3328–3342.

Takada, M., Tokuno, H., Hamada, I., Inase, M., Ito, Y., Imanishi, M., Hasegawa, N., Akazawa, T., Hatanaka, N., and Nambu, A. (2001). Organization of

inputs from cingulate motor areas to basal ganglia in macaque monkey. *Eur. J. Neurosci.* 14, 1633–1650.

Takada, M., Tokuno, H., Nambu, A., and Inase, M. (1998a). Corticostriatal input zones from the supplementary motor area overlap those from the contra- rather than ipsilateral primary motor cortex. *Brain Res.* 791, 335–340.

Takada, M., Tokuno, H., Nambu, A., and Inase, M. (1998b). Corticostriatal projections from the somatic motor areas of the frontal cortex in the macaque monkey: segregation versus overlap of input zones from the primary motor cortex, the supplementary motor area, and the premotor cortex. *Exp. Brain Res.* 120, 114–128.

Tepper, J. M., Wilson, C. J., and Koos, T. (2008). Feedforward and feedback inhibition in neostriatal GABAergic spiny neurons. *Brain Res. Rev.* 58, 272–281.

Tokuno, H., Inase, M., Nambu, A., Akazawa, T., Miyachi, S., and Takada, M. (1999). Corticostriatal projections from distal and proximal forelimb representations of the monkey primary motor cortex. *Neurosci. Lett.* 269, 33–36.

Vitek, J. L., Ashe, J., DeLong, M. R., and Alexander, G. E. (1994). Physiologic properties and somatotopic organization of the primate motor thalamus. *J. Neurophysiol.* 71, 1498–1513.

Vitek, J. L., Ashe, J., DeLong, M. R., and Kaneoke, Y. (1996). Microstimulation of primate motor thalamus: somatotopic organization and differential distribution of evoked motor responses among subnuclei. *J. Neurophysiol.* 75, 2486–2495.

Vitek, J. L., Chockkan, V., Zhang, J. Y., Kaneoke, Y., Evatt, M., DeLong, M. R., Triche, S., Mewes, K., Hashimoto, T., and Bakay, R. A. (1999). Neuronal activity in the basal ganglia in patients with generalized dystonia and hemiballismus. *Ann. Neurol.* 46, 22–35.

Wichmann, T., Bergman, H., and DeLong, M. R. (1994). The primate subthalamic nucleus. I. Functional properties in intact animals. *J. Neurophysiol.* 72, 494–506.

Wichmann, T., and Kliem, M. A. (2004). Neuronal activity in the primate substantia nigra pars reticulata during the performance of simple and memory-guided elbow movements. *J. Neurophysiol.* 91, 815–827.

Yelnik, J., Percheron, G., and Francois, C. (1984). A Golgi analysis of the primate globus pallidus. II. Quantitative morphology and spatial orientation of dendritic arborizations. *J. Comp. Neurol.* 227, 200–213.

Yoshida, S., Nambu, A., and Jinnai, K. (1993). The distribution of the globus pallidus neurons with input from various cortical areas in the monkeys. *Brain Res.* 611, 170–174.

Conflict of Interest Statement: The author declares that the research was conducted in the absence of any commercial or financial relationships that could be construed as a potential conflict of interest.

Received: 31 August 2010; accepted: 31 March 2011; published online: 20 April 2011.

Citation: Nambu A (2011) Somatotopic organization of the primate basal ganglia. Front. Neuroanat. 5:26. doi: 10.3389/fnana.2011.00026

frontiers in
SYSTEMS NEUROSCIENCE

ORIGINAL RESEARCH ARTICLE
published: 28 November 2011
doi: 10.3389/fnsys.2011.00089

Reduced pallidal output causes dystonia

Atsushi Nambu[1]*, Satomi Chiken[1], Pullanipally Shashidharan[2], Hiroki Nishibayashi[3], Mitsuhiro Ogura[3], Koji Kakishita[3], Satoshi Tanaka[3], Yoshihisa Tachibana[1], Hitoshi Kita[4] and Toru Itakura[3]

[1] Division of System Neurophysiology, National Institute for Physiological Sciences and Department of Physiological Sciences, Graduate University for Advanced Studies, Okazaki, Japan
[2] Department of Neurology, Mount Sinai School of Medicine, New York, NY, USA
[3] Department of Neurological Surgery, Wakayama Medical University, Wakayama, Japan
[4] Department of Anatomy and Neurobiology, College of Medicine, University of Tennessee Health Science Center, Memphis, TN, USA

Edited by:
Charles J. Wilson, University of Texas at San Antonio, USA

Reviewed by:
Thomas Wichmann, Emory University, USA
Jose Obeso, Universidad de Navarra, Spain

Correspondence:
Atsushi Nambu, Division of System Neurophysiology, National Institute for Physiological Sciences, 38 Nishigonaka, Myodaiji, Okazaki 444-8585, Japan.
e-mail: nambu@nips.ac.jp

Dystonia is a neurological disorder characterized by sustained or repetitive involuntary muscle contractions and abnormal postures. In the present article, we will introduce our recent electrophysiological studies in hyperkinetic transgenic mice generated as a model of DYT1 dystonia and in a human cervical dystonia patient, and discuss the pathophysiology of dystonia on the basis of these electrophysiological findings. Recording of neuronal activity in the awake state of DYT1 dystonia model mice revealed reduced spontaneous activity with bursts and pauses in both internal (GPi) and external (GPe) segments of the globus pallidus. Electrical stimulation of the primary motor cortex evoked responses composed of excitation and subsequent long-lasting inhibition, the latter of which was never observed in normal mice. In addition, somatotopic arrangements were disorganized in the GPi and GPe of dystonia model mice. In a human cervical dystonia patient, electrical stimulation of the primary motor cortex evoked similar long-lasting inhibition in the GPi and GPe. Thus, reduced GPi output may cause increased thalamic and cortical activity, resulting in the involuntary movements observed in dystonia.

Keywords: dystonia, globus pallidus, extracellular recording, stereotactic surgery, movement disorders

INTRODUCTION

Dystonia is a neurological disorder characterized by sustained or repetitive involuntary muscle contractions and abnormal postures. The pathophysiology of dystonia is poorly understood. No consistent neuropathological or biochemical changes have been detected yet. On the other hand, abnormal neuronal activity in the basal ganglia has been reported during stereotactic surgery for deep brain stimulation (DBS) in dystonia patients (Vitek et al., 1999; Zhuang et al., 2004; Starr et al., 2005; Tang et al., 2007).

In the present article, we will introduce our recent electrophysiological studies in hyperkinetic transgenic mice generated as a model of DYT1 dystonia (Chiken et al., 2008) and in a human cervical dystonia patient (Nishibayashi et al., 2011), and discuss the pathophysiology of dystonia on the basis of these electrophysiological findings. Firstly, we investigated the neuronal activity in the entopeduncular nucleus and globus pallidus in transgenic model mice of DYT1 dystonia (Chiken et al., 2008), the most common type of human primary generalized dystonia. Secondly, we also had a chance to record neuronal activity in the internal (GPi) and external (GPe) segments of the globus pallidus of a human cervical dystonia patient during stereotactic surgery (Nishibayashi et al., 2011). The entopeduncular nucleus and globus pallidus in rodents correspond to the GPi and GPe in primates, respectively, and thus, we will call these nuclei GPi and GPe hereafter. The GPi and GPe are two important nuclei in the basal ganglia circuitry, and their abnormal neuronal activity has been reported in movement disorders. We paid special attention to the responses of GPi and GPe neurons evoked by cortical stimulation. In voluntary movements, activity originating in the cortex is transmitted through the basal ganglia circuitry and finally reaches the output station of the basal ganglia, i.e., the GPi. Cortical stimulation can mimic information processing through the basal ganglia circuitry (Nambu et al., 2002; Tachibana et al., 2008). Motor cortical stimulation typically induces triphasic responses composed of early excitation, inhibition, and late excitation in GPi and GPe neurons of normal monkeys and rodents (Yoshida et al., 1993; Nambu et al., 2000; Chiken and Tokuno, 2003). The origin of each component has been identified, with the amplitudes and durations reflecting neuronal activity of the corresponding basal ganglia pathways and nuclei. In the studies by Chiken et al. (2008) and Nishibayashi et al. (2011), long-lasting inhibition was evoked in the GPi and GPe of both DYT1 dystonia model mice and a human cervical dystonia patient.

MATERIALS AND METHODS

ANIMAL STUDY

The DYT1 gene on chromosome 9q34 codes the torsinA protein (Ozelius et al., 1997). A three-base pair (GAG) deletion in the DYT1 gene, resulting in the loss of a glutamic acid residue (ΔE) in the torsinA protein (Ozelius et al., 1997), causes human DYT1 dystonia. Recently, Shashidharan et al. (2005) generated a transgenic mouse model by overexpression of human ΔE-torsinA. These transgenic mice developed hyperkinesia and rapid bidirectional circling. They also exhibited abnormal involuntary movements with dystonic-appearing self-clasping of limbs and head-shaking.

In the study by Chiken et al. (2008), six DYT1 dystonia model (5–28 weeks old, both male and female) and six age-matched normal mice were used. The experimental protocols were approved by the Animal Care and Use Committees of the Mount Sinai School of Medicine and the National Institutes of Natural Sciences, and all experiments were conducted according to the guidelines of the National Institutes of Health Guide for the Care and Use of Laboratory Animals. Each mouse was anesthetized with ketamine hydrochloride (100 mg/kg body weight, i.p.) and xylazine hydrochloride (4–5 mg/kg, i.p.), and fixed in a conventional stereotaxic apparatus. The skull was widely exposed. The exposed skull was completely covered with transparent acrylic resin, and then a small U-frame made of acetal resin for head fixation was mounted and fixed on the head of the mouse.

After recovery from the first surgery (2 or 3 days later), the mouse was positioned in a stereotaxic apparatus with its head restrained using the U-frame head holder under light anesthesia with ketamine hydrochloride (30–50 mg/kg, i.p.). A part of the skull in one hemisphere was removed to access the motor cortex, GPi, and GPe. Two pairs of bipolar stimulating electrodes (tip distance, 300–400 μm) made of 50-μm-diameter Teflon-coated tungsten wires were inserted into the primary motor cortex, one into the caudal forelimb region and the other into the orofacial region. These regions were confirmed by observing movements evoked by intracortical microstimulation. Stimulating electrodes were then fixed therein using acrylic resin.

After full recovery from the second surgery, the mouse was positioned in a stereotaxic apparatus with its head restrained painlessly using the U-frame head holder. The mouse lay down quietly in the awake state. For single unit recording of GPi and GPe neurons, a glass-coated Elgiloy-alloy microelectrode (0.8–1.5 MΩ at 1 kHz) was inserted vertically into the brain through the dura mater using a hydraulic microdrive. Signals from the electrode were amplified, converted to digital pulses using a window discriminator, and sampled using a computer. Spontaneous discharges were recorded, and spontaneous discharge rates and autocorrelograms (bin width of 0.5 ms) of the neurons were calculated from continuous digitized recordings for 30 s. Electrical stimulation of the primary motor cortex (200 μs duration single pulse, 20–50 μA strength), which induced muscle twitches in the corresponding body parts, was delivered. Similar intensities were used for dystonia model and normal mice. Responses to cortical stimulation were examined by constructing peristimulus time histograms (PSTHs; bin width of 1 ms) for 100 stimulus trials.

HUMAN STUDY

In the study by Nishibayashi et al. (2011), one cervical dystonia patient received stereotactic surgery for DBS electrode implantation into the bilateral GPi. The patient was 62-year-old female, and had a disease duration of 32 months, and a Toronto western spasmodic torticollis rating scale (TWSTRS) score of 54. Microelectrode recordings were performed to identify the targets. In addition, 10 Parkinson's disease patients [eight male and two female; mean age, 61.9 years; mean disease duration, 126 months; mean levodopa dosage, 460 mg/day; preoperative unified Parkinson's disease rating scale (UPDRS), 25.3 (best)–66.6 (worst)] were also investigated for comparison. Medications were withdrawn 18 h before operation in most patients. This study was approved by the ethical committee of Wakayama Medical University and followed its guidelines.

Surgery including microelectrode recordings was performed under local anesthesia. Burr holes were made bilaterally on the coronal suture about 30 mm lateral from the midline. After dural incision, a strip electrode with four platinum discs (5-mm-diameter) spaced 10 mm apart (Unique Medical, Tokyo, Japan) was inserted into the subdural space in the posterolateral direction, and placed on the upper limb region of the primary motor cortex ipsilateral to the target GPi. Electrical stimulation (1.0 ms duration single pulse, 1–20 mA strength at 1 Hz) was delivered through two of the four discs. A pair of discs inducing muscle twitches in the contralateral upper limb at the lowest intensity was selected. In the following recordings, stimulation was delivered through this pair at an intensity inducing clear muscle twitches (4–16 mA) at 1 Hz. A microelectrode (FC1002, Medtronic, Minneapolis, MN, USA) was inserted through the same burr hole targeting the tentative target in the posteroventral GPi, which was determined on the basis of magnetic resonance imaging (MRI). Neuronal activity was amplified, displayed (Leadpoint 9033A0315, Medtronic), and fed to a computer for online analysis. The responses induced by electrical stimulation of the cortex were assessed by constructing PSTHs (bin width of 1 ms) for 20–120 stimulus trials. Spontaneous discharge rates and patterns were analyzed from autocorrelograms (bin width of 0.5 ms) constructed from continuous digitized recordings for 50 s. On the basis of the microelectrode recordings, DBS electrodes (Model 3387, Medtronic) were implanted bilaterally into the GPi.

RESULTS

SPONTANEOUS ACTIVITY OF GPi AND GPe NEURONS IN DYT1 DYSTONIA MODEL MICE

GPi (50.6 ± 15.7 Hz, mean ± SD, $n = 94$; **Figure 1A**) and GPe (54.5 ± 16.3 Hz, $n = 70$) neurons in normal mice fired continuously at a high discharge rate. Traces of digitized spikes and autocorrelograms indicated that GPi (**Figures 1A,B**) and GPe neurons fired irregularly in normal mice. On the other hand, the firing frequency of GPi (27.8 ± 19.1 Hz, $n = 90$; **Figure 1C**) and GPe (35.4 ± 19.0 Hz, $n = 204$) neurons in DYT1 dystonia model mice was significantly lower than that in normal mice (**Figure 1E**; $p < 0.001$, Mann–Whitney U test). Discharge patterns also differed in dystonia model mice (**Figures 1C,D**). Bursts and pauses were frequently observed in GPi (thick black lines and thick white lines in **Figure 1C**) and GPe neurons of dystonia model mice.

RESPONSES OF GPi AND GPe NEURONS TO CORTICAL STIMULATION IN DYT1 DYSTONIA MODEL MICE

Cortical stimulation typically evoked a triphasic response composed of early excitation, followed by inhibition, and late excitation in GPi (**Figure 2A**) and GPe neurons of normal mice. On the other hand, the most common response pattern of GPi (56%) and GPe (41%) neurons in dystonia model mice was short-latency monophasic or biphasic excitation followed by long-lasting inhibition (**Figure 2B**), a pattern never observed in normal mice. The duration of the long-lasting inhibition was 73.7 ± 29.4 ms in the GPi ($n = 29$) and 66.7 ± 31.3 ms in the GPe ($n = 46$).

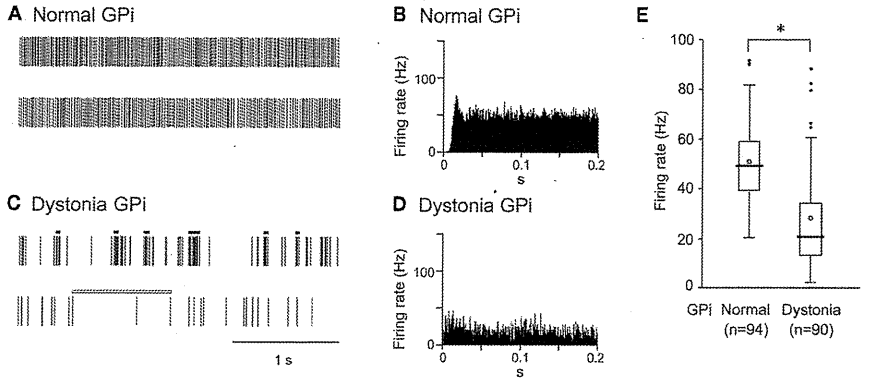

FIGURE 1 | Spontaneous activity of neurons in the internal segment of the globus pallidus (GPi) in DYT1 dystonia model mice. (A,C) Spikes are shown as digital signals in normal **(A)** and dystonia model **(C)** mice. Bursts and pauses in the digital signals are indicated by horizontal black thick lines and horizontal white thick lines, respectively. **(B,D)** Auto-correlograms are shown in normal **(B)** and dystonia model **(D)** mice. **(E)** Box plots of firing rates in normal (left) and dystonia model (right) mice. The boxes are constructed with the top line bounding the upper quartile and the bottom line bounding the lower quartile. The median and mean excluding outliers are indicated by a thick horizontal line and an open circle in the box, respectively. The short horizontal lines show the largest and smallest values that are not outliers. Outliers are shown as small closed circles. *, significantly different ($p < 0.001$, Mann–Whitney U test). Modified from Chiken et al. (2008).

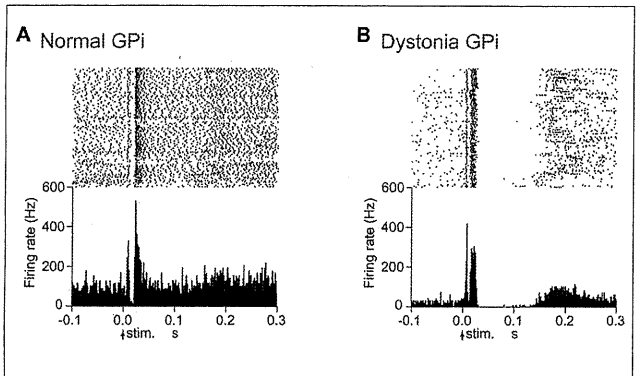

FIGURE 2 | Responses of GPi neurons to cortical stimulation in DYT1 dystonia model mice. (A) Raster and peristimulus time histograms (PSTHs) for normal mice. Cortical stimuli were delivered at time 0 (arrows) for 100 trials. **(B)** Raster and PSTHs for dystonia model mice. Abnormal responses with long-lasting inhibition were observed. Modified from Chiken et al. (2008).

SOMATOTOPIC ORGANIZATION OF THE GPi AND GPe IN DYT1 DYSTONIA MODEL MICE

Stimulation of both forelimb and orofacial regions of the motor cortex was performed. By observing cortically evoked responses, cortical regions projecting to each GPi neuron could be identified. In normal mice, many neurons responded to stimulation of the forelimb region, and a small number of neurons responded to stimulation of the orofacial region (**Figure 3A**). The number of neurons with convergent inputs from both forelimb and orofacial regions was small (7%). On the other hand, the number of GPi neurons with convergent inputs was increased in dystonia model mice (28%).

The locations of recorded GPi neurons are plotted on the basis of cortical inputs in **Figure 3B**. In the GPi of normal mice, the neurons with forelimb inputs were distributed over a wide area of the GPi, although not in its most medial portion (**Figure 3B** top). A few neurons with orofacial inputs were found in the lateral portion of the GPi. In dystonia model mice, however, such a segregation disappeared. The number of GPi neurons with orofacial inputs and those with convergent inputs was increased, and they intruded into the central portion of the GPi, although the most medial portion remained unresponsive (**Figure 3B** bottom). Similar changes were also observed in the GPe. These observations suggest that somatotopic arrangements are disorganized in the GPi and GPe of dystonia model mice.

ACTIVITY OF GPi AND GPe NEURONS IN A HUMAN CERVICAL DYSTONIA PATIENT

Neurons were recorded mostly in motor territories of the GPi and GPe. The firing rates of GPi (62.3 ± 12.1 Hz, $n = 9$) and GPe (45.8 ± 17.6 Hz, $n = 11$) neurons in a cervical dystonia patient were significantly lower than those of GPi (92.7 ± 40.1 Hz, $n = 34$) and GPe (81.0 ± 52.5 Hz, $n = 17$) neurons in Parkinsonian patients ($p < 0.05$, t-test). Most GPi and GPe neurons of a cervical dystonia patient showed burst (6/9 GPi and 5/11 GPe) or oscillatory (1–4 Hz) burst (1/9 GPi and 6/11 GPe) activity (**Figure 4A**). More than one-third of recorded neurons (6/13 GPi and 4/11 GPe in a cervical dystonia patient and 21/68 GPi and 18/45 GPe in Parkinsonian patients) showed responses to cortical stimulation. These GPi and GPe neurons were considered to be located in the upper limb regions of the GPi and GPe, because these neurons often responded to sensory stimulation of the upper limb. In Parkinsonian patients, response patterns to cortical stimulation were combinations of early excitation, inhibition, and late excitation (data not shown). On the other hand, in a cervical dystonia patient, long-lasting inhibition preceded by excitation (**Figure 4B**) and long-lasting monophasic inhibition (**Figure 4C**) were the typical response patterns. These response patterns are very similar to those observed in dystonia model mice (compare **Figures 4B,C** with **Figure 2B**).

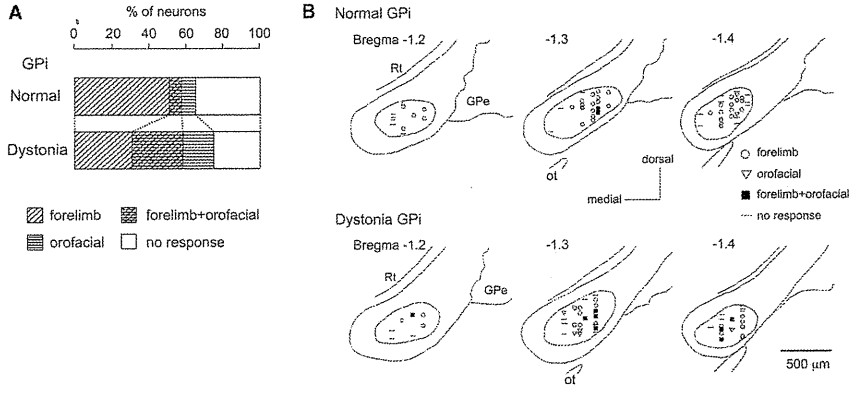

FIGURE 3 | Somatotopic organization in the GPi of DYT1 dystonia model mice. (A) Proportions of neurons classified on the basis of cortical inputs in normal (top) and dystonia model (bottom) mice. **(B)** Distribution of recorded GPi neurons indicated by symbols on the basis of cortical inputs. Data from normal (top) and dystonia model (bottom) mice are shown in frontal sections. Figures in the left upper corner represent distance from bregma. GPe, external segment of the globus pallidus; Rt, reticular thalamic nucleus; Ot, optic tract. Modified from Chiken et al. (2008).

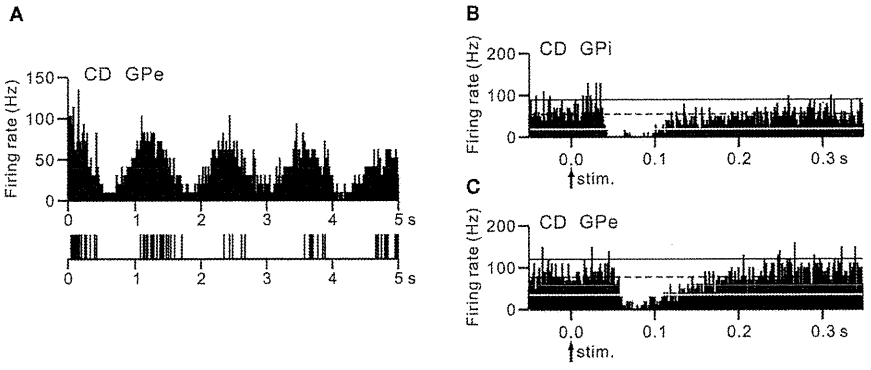

FIGURE 4 | Activity of GPi and GPe neurons in a human cervical dystonia patient. (A) Autocorrelograms and slow traces of digitized spikes of GPe neurons recorded from a cervical dystonia (CD) patient. **(B,C)** PSTHs (bin width of 1 ms) showing the responses of GPi **(B)** and GPe **(C)** neurons evoked by stimulation of the upper limb region of the primary motor cortex in a cervical dystonia patient. Cortical stimuli were delivered at time 0 (arrows) for 100 trials. The mean firing rate is indicated by black dotted lines. The statistical levels of $p < 0.05$ (one-tailed *t*-test) calculated from the firing rate during 100 ms preceding the onset of stimulation are indicated by black and white solid lines (upper and lower limits of $p < 0.05$). Modified from Nishibayashi et al. (2011).

DISCUSSION

The first part of the present article characterized the electrophysiological properties of transgenic mice developed to express human ΔE-torsinA as a model of DYT1 dystonia. These mice exhibited: (1) decreased GPi and GPe activity with bursts and pauses, (2) cortically evoked long-lasting inhibition in the GPi and GPe, and (3) somatotopic disorganization in the GPi and GPe. In the second part, similar activity changes, such as decreased activity with bursts and cortically evoked long-lasting inhibition, were also observed in the GPi and GPe of a human cervical dystonia patient. These neuronal abnormalities may be responsible for the symptoms observed in dystonia.

DECREASED GPi AND GPe ACTIVITY IN DYSTONIA

In the present article, reduction of the spontaneous firing rates of GPi and GPe neurons was observed in dystonia model mice and a human cervical dystonia patient. Alteration of firing patterns was also observed in both of them, including bursting discharges and pauses. Decreased discharge rates and irregularly grouped discharges with intermittent pauses in GPi and GPe neurons were also reported in patients with generalized dystonia (Vitek et al., 1999; Zhuang et al., 2004; Starr et al., 2005) and cervical dystonia (Tang et al., 2007). Dystonic hamsters with paroxysmal generalized dystonia also exhibited reduced and bursting GPi activity (Gernert et al., 2002). The correlation between abnormal neuronal activity and abnormal movements was not investigated in the present mice study, because it was difficult to observe abnormal movements under head fixation. The mechanisms responsible for decreased firing rates may include: (1) alteration of membrane properties of GPi and GPe neurons, (2) increased inhibitory inputs to the GPi and GPe, such as GABAergic inputs from the striatum, and/or (3) decreased excitatory inputs to the GPi and

GPe, such as glutamatergic inputs from the subthalamic nucleus (STN). Inhibitory inputs from the striatum to the GPi and GPe were increased in dystonia model mice as discussed in the next section.

CORTICALLY EVOKED LONG-LASTING INHIBITION IN GPi AND GPe NEURONS OF DYSTONIA

In normal mice, cortical stimulation typically induced triphasic responses composed of early excitation, inhibition, and late excitation in GPi and GPe neurons. Similar triphasic responses were also observed in the GPi and GPe of rats and monkeys. The origin of each component has been intensively studied (Ryan and Clark, 1991; Maurice et al., 1998, 1999; Nambu et al., 2000; Kita et al., 2004; Tachibana et al., 2008). Early excitation is mediated by the cortico-STN-GPe/GPi pathway, while inhibition and late excitation are mediated by the cortico-striato-GPe/GPi and cortico-striato-GPe-STN-GPe/GPi pathways, respectively.

On the other hand, in dystonia model mice we examined, cortical stimulation induced early excitation followed by late long-lasting inhibition in GPi and GPe neurons. Similar response patterns were induced in GPi and GPe neurons of a human cervical dystonia patient. These abnormal patterns of responses may be generated through the cortico-basal ganglia pathways. The early excitation seems to be mediated, at least in its early phase, by the cortico-STN-GPe/GPi pathway, as in normal mice, since the latency of the early excitation in dystonia model mice was short and similar to that in normal mice. The origin of the late long-lasting inhibition may be (1) increased inhibitory input via the striato-GPe/GPi pathway, or (2) decreased excitatory input via the STN-GPe/GPi pathway. The latter explanation seems less likely to be correct, since our preliminary observation indicates that the spontaneous activity of STN neurons is unchanged in dystonia model mice. Thus, increased activity through both cortico-striato-GPi *direct* and cortico-striato-GPe *indirect* pathways is considered to be the fundamental change in dystonia. The above observations also suggest that spontaneous excitation in the cortex that is transmitted to the GPi and GPe through the cortico-basal ganglia pathways could also induce short-latency excitation and long-lasting inhibition, which might be the origins of bursts and pauses, respectively.

SOMATOTOPIC DISORGANIZATION IN THE GPi AND GPe OF DYSTONIA

The somatotopic organization in the GPi and GPe was observed in normal mice as well as monkeys (DeLong et al., 1985; Yoshida et al., 1993). On the other hand, in dystonia model mice, somatotopic arrangements were disorganized, and many GPi and GPe neurons received convergent inputs from both forelimb and orofacial regions. Widened somatosensory receptive fields in pallidal neurons were reported in patients with generalized (Vitek et al., 1999) and focal (Lenz et al., 1998; Sanger et al., 2001) dystonia. Interference of information processing may occur through the cortico-basal ganglia pathways. One explanation for this could be that each single GPi or GPe neuron receives inputs from more striatal neurons in dystonia model mice than in normal mice. Such an explanation agrees well with the hypothesis that in dystonia, inhibition in the GPi/GPe is increased through the striato-GPe/GPi pathways as described in the previous section.

PATHOPHYSIOLOGY OF DYSTONIA

The GPi, the output nucleus of the basal ganglia, is composed of GABAergic inhibitory neurons and fires at high frequency in normal states. Its target structures, such as the thalamus and frontal cortex, are thus continuously inhibited. Striatal inputs reduce GPi activity in a temporal fashion, excite thalamic and cortical neurons through disinhibitory mechanism, and finally release appropriate movements with appropriate timing (**Figure 5A**; Nambu et al., 2000, 2002). On the other hand, in dystonia model mice and a human cervical dystonia patient, cortical excitation induced long-lasting inhibition in the GPi (**Figure 5B**). This suggests that even tiny amounts of spontaneous or voluntary neuronal activity originating in the cortex are transmitted through the cortico-basal ganglia pathways to induce strong, long-lasting inhibition in the GPi. Moreover, somatotopic disorganization was noted in the GPi of dystonia, and cortical activation could induce inhibition over a wide area of the GPi. Reduced GPi output may activate wide areas of the thalamus and cortex in an uncontrollable fashion, resulting in the involuntary movements observed in dystonia. In a similar manner, the cortical areas controlling agonist and antagonist muscles are concurrently activated, and co-contraction of agonist and antagonist muscles could be induced. This may also explain the "motor overflow" that is unintentional muscle contraction during voluntary movements in dystonia. Activation of the upper limb region in the motor cortex, for example, may inhibit large areas of the GPi and finally induce involuntary movements of multiple body parts (**Figure 5B**).

CONCLUSION

The activity of GPi and GPe neurons in DYT1 dystonia model mice and a human cervical dystonia patient was investigated. Both of them showed similar activity changes, such as decreased spontaneous activity with bursts and long-lasting inhibition evoked by cortical stimulation, indicating increased activity through

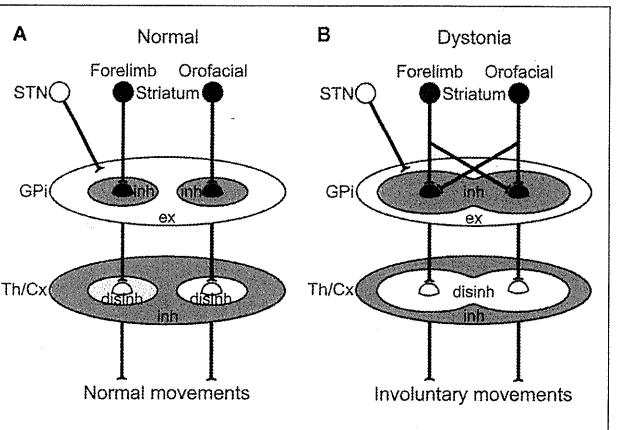

FIGURE 5 | Schematic diagrams showing information processing through the basal ganglia in normal (A) and dystonia (B) conditions. In dystonia **(B)**, cortical activation induces strong inhibition over a wide area of the GPi. Reduced GPi output may cause strong excitation in the thalamus (Th) and cortex (Cx) through disinhibitory mechanism, resulting in the involuntary movements. disinh, disinhibition; ex, excitation; inh, inhibition; STN, subthalamic nucleus. Modified from Chiken et al. (2008).

the cortico-striato-GPi *direct* and cortico-striato-GPe *indirect* pathways. Such a mechanism may explain the pathophysiology of dystonia: Neuronal activity originating in the cortex is transmitted through the cortico-basal ganglia pathways to induce strong, long-lasting inhibition in the GPi. Reduced GPi output may cause increased thalamic and cortical activity, resulting in the involuntary movements.

ACKNOWLEDGMENTS

The animal study was supported by a Grants-in-Aid for Exploratory Research (18650089) and a Grants-in-Aid for Scientific Research (B) (18300135) from the Ministry of Education, Culture, Sports, Science, and Technology of Japan (MEXT), The Uehara Memorial Foundation, Takeda Science Foundation, and United States–Japan Brain Research Cooperative Program (Atsushi Nambu); a Grants-in-Aid for Scientific Research (C) (19500354) from MEXT (Satomi Chiken); and National Institute of Neurological Disorders and Stroke-National Institutes of Health Grant (NS-043038) (Pullanipally Shashidharan). The human study was supported by Wakayama Foundation for the Promotion of Medicine (Toru Itakura), a Grants-in-Aid for Scientific Research (B) (18300135) from MEXT and the Uehara Memorial Foundation (Atsushi Nambu), and NIH grants (NS-47085 and NS-57236) (Hitoshi Kita).

REFERENCES

Chiken, S., Shashidharan, P., and Nambu, A. (2008). Cortically evoked long-lasting inhibition of pallidal neurons in a transgenic mouse model of dystonia. *J. Neurosci.* 28, 13967–13977.

Chiken, S., and Tokuno, H. (2003). Ablation of striatal interneurons influences activities of entopeduncular neurons. *Neuroreport* 14, 675–678.

DeLong, M. R., Crutcher, M. D., and Georgopoulos, A. P. (1985). Primate globus pallidus and subthalamic nucleus: functional organization. *J. Neurophysiol.* 53, 530–543.

Gernert, M., Bennay, M., Fedrowitz, M., Rehders, J. H., and Richter, A. (2002). Altered discharge pattern of basal ganglia output neurons in an animal model of idiopathic dystonia. *J. Neurosci.* 22, 7244–7253.

Kita, H., Nambu, A., Kaneda, K., Tachibana, Y., and Takada, M. (2004). Role of ionotropic glutamatergic and GABAergic inputs on the firing activity of neurons in the external pallidum in awake monkeys. *J. Neurophysiol.* 92, 3069–3084.

Lenz, F. A., Suarez, J. I., Metman, L. V., Reich, S. G., Karp, B. I., Hallett, M., Rowland, L. H., and Dougherty, P. M. (1998). Pallidal activity during dystonia: somatosensory reorganisation and changes with severity. *J. Neurol. Neurosurg. Psychiatr.* 65, 767–770.

Maurice, N., Deniau, J. M., Glowinski, J., and Thierry, A. M. (1998). Relationships between the prefrontal cortex and the basal ganglia in the rat: physiology of the corticosubthalamic circuits. *J. Neurosci.* 18, 9539–9546.

Maurice, N., Deniau, J. M., Glowinski, J., and Thierry, A. M. (1999). Relationships between the prefrontal cortex and the basal ganglia in the rat: physiology of the cortico-nigral circuits. *J. Neurosci.* 19, 4674–4681.

Nambu, A., Tokuno, H., Hamada, I., Kita, H., Imanishi, M., Akazawa, T., Ikeuchi, Y., and Hasegawa, N. (2000). Excitatory cortical inputs to pallidal neurons via the subthalamic nucleus in the monkey. *J. Neurophysiol.* 84, 289–300.

Nambu, A., Tokuno, H., and Takada, M. (2002). Functional significance of the cortico-subthalamo-pallidal 'hyperdirect' pathway. *Neurosci. Res.* 43, 111–117.

Nishibayashi, H., Ogura, M., Kakishita, K., Tanaka, S., Tachibana, Y., Nambu, A., Kita, H., and Itakura, T. (2011). Cortically evoked responses of human pallidal neurons recorded during stereotactic neurosurgery. *Mov. Disord.* 26, 469–476.

Ozelius, L. J., Hewett, J. W., Page, C. E., Bressman, S. B., Kramer, P. L., Shalish, C., de Leon, D., Brin, M. F., Raymond, D., Corey, D. P., Fahn, S., Risch, N. J., Buckler, A. J., Gusella, J. F., and Breakefield, X. O. (1997). The early-onset torsion dystonia gene (DYT1) encodes an ATP-binding protein. *Nat. Genet.* 17, 40–48.

Ryan, L. J., and Clark, K. B. (1991). The role of the subthalamic nucleus in the response of globus pallidus neurons to stimulation of the prelimbic and agranular frontal cortices in rats. *Exp. Brain Res.* 86, 641–651.

Sanger, T. D., Tarsy, D., and Pascual-Leone, A. (2001). Abnormalities of spatial and temporal sensory discrimination in writer's cramp. *Mov. Disord.* 16, 94–99.

Shashidharan, P., Sandu, D., Potla, U., Armata, I. A., Walker, R. H., McNaught, K. S., Weisz, D., Sreenath, T., Brin, M. F., and Olanow, C. W. (2005). Transgenic mouse model of early-onset DYT1 dystonia. *Hum. Mol. Genet.* 14, 125–133.

Starr, P. A., Rau, G. M., Davis, V., Marks, W. J. Jr., Ostrem, J. L., Simmons, D., Lindsey, N., and Turner, R. S. (2005). Spontaneous pallidal neuronal activity in human dystonia: comparison with Parkinson's disease and normal macaque. *J. Neurophysiol.* 93, 3165–3176.

Tachibana, Y., Kita, H., Chiken, S., Takada, M., and Nambu, A. (2008). Motor cortical control of internal pallidal activity through glutamatergic and GABAergic inputs in awake monkeys. *Eur. J. Neurosci.* 27, 238–253.

Tang, J. K., Moro, E., Mahant, N., Hutchison, W. D., Lang, A. E., Lozano, A. M., and Dostrovsky, J. O. (2007). Neuronal firing rates and patterns in the globus pallidus internus of patients with cervical dystonia differ from those with Parkinson's disease. *J. Neurophysiol.* 98, 720–729.

Vitek, J. L., Chockkan, V., Zhang, J. Y., Kaneoke, Y., Evatt, M., DeLong, M. R., Triche, S., Mewes, K., Hashimoto, T., and Bakay, R. A. E. (1999). Neuronal activity in the basal ganglia in patients with generalized dystonia and hemiballismus. *Ann. Neurol.* 46, 22–35.

Yoshida, S., Nambu, A., and Jinnai, K. (1993). The distribution of the globus pallidus neurons with input from various cortical areas in the monkeys. *Brain Res.* 611, 170–174.

Zhuang, P., Li, Y., and Hallett, M. (2004). Neuronal activity in the basal ganglia and thalamus in patients with dystonia. *Clin. Neurophysiol.* 115, 2542–2557.

Conflict of Interest Statement: The authors declare that the research was conducted in the absence of any commercial or financial relationships that could be construed as a potential conflict of interest.

Received: 21 April 2011; accepted: 18 October 2011; published online: 28 November 2011.

Citation: Nambu A, Chiken S, Shashidharan P, Nishibayashi H, Ogura M, Kakishita K, Tanaka S, Tachibana Y, Kita H and Itakura T (2011) Reduced pallidal output causes dystonia. Front. Syst. Neurosci. 5:89. doi: 10.3389/fnsys.2011.00089

J Neuropathol Exp Neurol

Vol. 70, No. 8
August 2011
pp. 686–697

ORIGINAL ARTICLE

Parkin-Mediated Protection of Dopaminergic Neurons in a Chronic MPTP-Minipump Mouse Model of Parkinson Disease

Toru Yasuda, PhD, Hideki Hayakawa, PhD, Tomoko Nihira, DMC, Yong-Ri Ren, PhD, Yasuto Nakata, MSc, Makiko Nagai, MD, PhD, Nobutaka Hattori, MD, PhD, Koichi Miyake, MD, PhD, Masahiko Takada, MD, PhD, Takashi Shimada, MD, PhD, Yoshikuni Mizuno, MD, PhD, and Hideki Mochizuki, MD, PhD

Abstract

Loss-of-function mutations in the ubiquitin ligase parkin are the major cause of recessively inherited early-onset Parkinson disease (PD). Impairment of parkin activity caused by nitrosative or dopamine-related modifications may also be responsible for the loss of dopaminergic (DA) neurons in sporadic PD. Previous studies have shown that viral vector-mediated delivery of parkin prevented DA neurodegeneration in several animal models, but little is known about the neuroprotective actions of parkin in vivo. Here, we investigated mechanisms of neuroprotection of overexpressed parkin in a modified long-term mouse model of PD using osmotic minipump administration of 1-methyl-4-phenyl-1,2,3,6-tetrahydropyridine (MPTP). Recombinant adeno-associated viral vector-mediated intranigral delivery of parkin prevented motor deficits and DA cell loss in the mice. Ser129-phosphorylated α-synuclein–immunoreactive cells were increased in the substantia nigra of parkin-treated mice. Moreover, delivery of parkin alleviated the MPTP-induced decrease of the active phosphorylated form of Akt. On the other hand, upregulation of p53 and mitochondrial alterations induced by chronic MPTP administration were barely suppressed by parkin. These results suggest that the neuroprotective actions of parkin may be impaired in severe PD.

From the Department of Neurology (TY, HH, TN, YRR, YN, MN, YM, HM), and Division of Neuroregenerative Medicine (YM), Kitasato University School of Medicine, Minami-ku, Sagamihara, Kanagawa, Japan; Department of Neurology, and Research Institute for Diseases of Old Age (TY, HH, TN, YRR, NH, YM, HM), Juntendo University School of Medicine, Bunkyo-ku, Tokyo, Japan; Department of Biochemistry and Molecular Biology (KM, TS), Division of Gene Therapy Research, Center for Advanced Medical Technology, Nippon Medical School, Bunkyo-ku, Tokyo, Japan; and Systems Neuroscience Section (MT), Department of Cellular and Molecular Biology, Primate Research Institute, Kyoto University, Inuyama, Aichi, Japan.

Send correspondence and reprint requests to: Hideki Mochizuki, MD, PhD, Department of Neurology, Kitasato University School of Medicine, 1-15-1 Kitasato, Minami-ku, Sagamihara, Kanagawa 252-0374, Japan; E-mail: hmoc0823@med.kitasato-u.ac.jp

This work was supported by the Program for Promotion of Fundamental Studies in Health Sciences of the National Institute of Biomedical Innovation; Grants-in-Aid from the Research Committee of CNS Degenerative Diseases, the Ministry of Health, Labour and Welfare of Japan (to H.M.); the Research Grant for Longevity Sciences from the Ministry of Health, Labour and Welfare of Japan (to H.M.); and grants (No. S0801035) from the Ministry of Education, Culture, Sports, Science, and Technology of Japan (to H.M.).

Supplemental digital content is available for this article. Direct URL citations appear in the printed text and are provided in the HTML and PDF versions of this article on the journal's Web site (www.jneuropath.com).

Key Words: α-Synuclein, Adeno-associated virus, MPTP, Neuroprotection, Osmotic minipump, Parkin, Parkinson disease.

INTRODUCTION

Parkinson disease (PD) is a progressive neurodegenerative disorder characterized clinically by resting tremor, rigidity, akinesia, and postural instability (1). The pathologic hallmarks of PD are loss of dopaminergic (DA) neurons in the substantia nigra (SN) pars compacta (SNpc) and intraneuronal protein inclusions termed *Lewy bodies*, which are composed mainly of α-synuclein (αSyn) (2). Both environmental and genetic factors are considered to be involved in PD pathogenesis (1, 3). Sporadic cases represent more than 90% of total patients with PD, but there are several inherited forms caused by mutations in single genes (1). Among these familial forms of PD, approximately 50% of recessively inherited early-onset parkinsonism is caused by loss-of-function mutations in the parkin gene *PARK2* (4).

PARK2 encodes a 465-amino acid protein that functions as a ubiquitin ligase (5). Most PARK2 patients seem to lack Lewy bodies (6–9), suggesting an important role for parkin in Lewy body formation (10). Several putative substrates of parkin have been reported and can be divided into 2 subgroups: those that are destined for proteasomal degradation by receiving canonical K48-linked polyubiquitination (11) and others that acquire multiple physiological or pathophysiological functions by receiving monoubiquitination or K63-linked polyubiquitination. The latter may be involved in inclusion formation (12–16). In animal models, loss of parkin increases mitochondrial dysfunction and oxidative damage (17), impairment of evoked dopamine release (18), and vulnerability to inflammation-related neurodegenerative insult (19). *S*-Nitrosylation or covalent binding of dopamine-related compounds may be responsible for parkin inactivation and subsequent DA cell death in sporadic PD (20–22). Moreover, there is increasing evidence that ectopically overexpressed parkin provides neuroprotective effects in genetic and environmental PD models, including *LRRK2*-transgenic (23) and *PINK1*-knockdown fruit flies (24), 6-hydroxydopamine–lesioned rats (25), and mice treated transiently with 1-methyl-4-phenyl-1,2,3,6-tetrahydropyridine (MPTP) (26). We previously reported that recombinant adeno-associated viral (rAAV) vector-mediated delivery of parkin

prevented αSyn-induced DA neuronal loss in rat and monkey brains (27, 28).

Recent studies indicate that there are functional interactions of parkin with PINK1, which is involved in mitochondrial quality control (29–33). However, the neuroprotective actions of parkin against long-term mitochondrial insult are relatively unknown in vivo. This study was designed to dissect the parkin-mediated neuroprotection in a long-term environmental model of PD. We generated modified high-dose and long-term MPTP mice using Alzet osmotic minipumps and investigated the impact of rAAV-mediated parkin delivery.

MATERIALS AND METHODS

Mice

Normal male C57BL/6J mice were purchased from Charles River Laboratories (Kanagawa, Japan). All experimental protocols were approved by the Ethics Review Committee for Animal Experimentation of Juntendo University and by the Animal Experimentation and Ethics Committee of the Kitasato University School of Medicine.

Preparation of rAAV Vector

The plasmid pAAV-MCS (CMV promoter; Stratagene, La Jolla, CA) carrying human *parkin* complementary DNA (named pAAV-MCS-parkin) or human *αSyn* complementary DNA (pAAV-MCS-αSyn) was constructed as previously reported (27, 34). High-titer serotype-1 rAAV (rAAV1) vector stocks were prepared using the plasmid pAAV-MCS-parkin, pAAV-MCS-αSyn, or pAAV-hrGFP (humanized recombinant green fluorescent protein; Stratagene), as described (28, 35). The rAAV1 vectors were purified by ultracentrifugation in a gradient density of OptiPrep solution (Axis-Shield PoC AS, Oslo, Norway), which was then removed by ultrafiltration using Centricon Plus-20 (10,000 MWCO; Millipore Corp, Temecula, CA). The titers of rAAV1 to produce parkin (named rAAV1-parkin), αSyn (rAAV1-αSyn), or hrGFP (rAAV1-hrGFP) were 5×10^{11} genomes per milliliter.

Stereotaxic Injection of rAAV1 Vectors

Mice were anesthetized with sodium pentobarbital (50 mg/kg body weight, intraperitoneally [i.p.]) and positioned in a stereotaxic frame. For immunohistochemistry (IHC) and measurement of the striatal dopamine and its metabolites, rAAV1 vector was injected unilaterally. For Western blotting, the rAAV1 vector was injected bilaterally. The skull was exposed, and a small portion of the skull over the SN was removed with a dental drill. Subsequently, the rAAV1 vector was injected into the SN (2 μL; 2.8 mm posterior and 1.3 mm lateral from the bregma, 4.4 mm below the dural surface; tooth bar = −2 mm) through a 5-μL Hamilton microsyringe, as previously described (35).

MPTP Infusion

The 13-week-old mice (~30 g body weight) were implanted i.p. with the Alzet osmotic minipumps (Model 2004, releasing rate = 0.25 μL/h, reservoir volume = 200 μL; Durect Corp, Cupertino, CA), filled with saline (control group), 250 mg/mL MPTP-HCl (50-mg/kg-per-day group; dissolved in saline; Sigma-Aldrich Corp, St Louis, MO), or 500 mg/mL MPTP-HCl (100-mg/kg-per-day group). For bolus injection, mice were injected i.p. with MPTP at 30 mg/kg per day for 5 consecutive days (designated as subacute; n = 4).

For rAAV1-injected mice, the same Alzet minipumps filled with saline (control group) or 250 mg/mL MPTP-HCl (50-mg/kg-per-day group) were implanted at 14 days after injection of the rAAV1 vectors. MPTP was handled in accordance with guidelines reported by Przedborski et al (36).

Behavioral Analysis

To evaluate behavioral changes, the mice were analyzed by a rotarod test 25 days after implantation of the osmotic minipump (i.e. 3 days before death). Mice were kept for 300 seconds twice on a rotarod apparatus accelerating from 0 to 32 rpm at 45-minute intervals (Model 7650, rota-rod for mice; Ugo Basile Biological Research Apparatus, Comerio VA, IT). The latency times (seconds) to fall were measured by accelerating from 0 to 32 rpm in 300 seconds.

rAAV1-injected mice were analyzed by apomorphine-induced rotation test 25 days after the minipump implantation (3 days before death). Mice were habituated in a circular chamber (16 cm in diameter) for 10 minutes. Then, after the injection of apomorphine-HCl (0.5 mg/kg i.p., dissolved in saline containing 30% ascorbic acid; Sigma-Aldrich Corp), rotation behavior was monitored for 40 minutes using a video recorder. In a previous report, apomorphine-challenged rats rotated toward the side with weaker DA neurotransmission (37), and the number of contralateral full body turns was

TABLE. Numbers of Mice Used for rAAV1 Injection Experiments

Immunohistochemistry and Other Studies	**Unilateral Injection of rAAV1 Vectors; Killed 28 Days After Minipump Implantation**			
Group	rAAV1-hrGFP/saline	rAAV1-parkin/saline	rAAV1-hrGFP/MPTP	rAAV1-parkin/MPTP
No. mice analyzed/injected	4/4	4/4	4/6	5/6
Western	**Bilateral Injection of rAAV1 Vectors; Killed 7 Days After Minipump Implantation**			
Group	rAAV1-hrGFP/saline	rAAV1-parkin/saline	rAAV1-hrGFP/MPTP	rAAV1-parkin/MPTP
No. mice analyzed/injected	4/4	4/4	4*/6	4*/6

Numbers of mice injected with the rAAV1 vector (injected) and used for data analyses (analyzed) are shown. For immunohistochemistry and measurements of dopamine and its metabolites, mice that exhibited foreign protein expression in more than ~80% of the area of the entire rostrocaudal region of the substantia nigra pars compacta were used for the analyses. In Western blotting analysis, the protein samples that showed an intense foreign protein expression were used for the analyses.

*One mouse died before minipump implantation.

hrGFP, humanized recombinant green fluorescent protein; MPTP, 1-methyl-4-phenyl-1,2,3,6-tetrahydropyridine; rAAV1, recombinant adeno-associated viral vector 1.

counted by playing back the recorded videotape. A full-body turn was defined as continuous and pivotal turning exceeding 180 degrees.

Tissue Processing

At 7 or 28 days after implantation of the minipumps, or 25 days after the first injection of MPTP (subacute group), mice were deeply anesthetized with sodium pentobarbital (250 mg/kg, i.p.) and perfused transcardially with phosphate-buffered saline (PBS). The brains were removed en bloc from the skull and cut coronally along the anterior tangent to the median eminence. The striatal tissues were then dissected and immediately frozen on dry ice. For Western blotting, the brain blocks including the entire rostrocaudal extent of the SN were cut coronally at 2-mm thickness (Figure, Supplemental Digital Content 1, parts A, B, http://links.lww.com/NEN/A252). After removal of the cortical and hippocampal tissues, the ventral midbrains were cut horizontally along the ventral end close to the SN to remove the tissues including the median eminence and pontine nucleus. Then, ventral parts of midbrain tissues (~1.2 mm from the ventral end) were dissected horizontally, from which the ventrolateral tissues including SN pars reticulata were removed (Figure, Supplemental Digital Content 1, parts A, B, http://links.lww.com/NEN/A252), and immediately frozen on dry ice. For IHC, the posterior parts of brain blocks, including the entire rostrocaudal extent of the SN, were fixed overnight in 4% paraformaldehyde in PBS and immersed in PBS containing 30% sucrose until sinking. Coronal sections of the SN were cut serially at 20-μm thickness by a cryostat (CM1900; Leica Microsystems, Wetzlar, Germany).

The rAAV1-αSyn-injected (n = 3) and rAAV1-hrGFP-injected mice (n = 3) were killed at 4 weeks after injection. Brain tissues including the entire rostrocaudal extent of the SN were fixed overnight in 4% paraformaldehyde in PBS and processed for IHC as described previously.

Antibodies

The primary antibodies used for IHC were rabbit anti-hrGFP (diluted at 1:500; Stratagene), rabbit anti-parkin (no. 2132; 1:500; Cell Signaling Technology, Inc, Danvers, MA), mouse anti-parkin (no. 4211, clone Park8; 1:200; Cell Signaling Technology), mouse anti-tyrosine hydroxylase (TH) (1:10000; Calbiochem, San Diego, CA), rabbit anti-TH (1:5000; Calbiochem), sheep anti-TH (1:1000; Calbiochem), mouse anti-glial fibrillary acidic protein (clone ab10062; 1:500; Abcam, Cambridge, MA), mouse anti-human αSyn (clone LB509; 1:200; Invitrogen Corp, Carlsbad, CA), rabbit anti–Ser129-phosphorylated αSyn (clone ab59264; 1:500; Abcam), and rabbit anti-translocase of the outer membrane 20 (Tom20) antibodies (FL-145; 1:500; Santa Cruz Biotechnology, Inc, Santa Cruz, CA).

The primary antibodies used for Western blotting were as follows: rabbit anti-hrGFP (1:500), mouse anti-parkin (1:500), rabbit anti–phospho-Akt (Ser473) (no. 4060, clone D9E; 1:1000; Cell Signaling Technology), rabbit anti-Akt (no. 9272; 1:500; Cell Signaling Technology), mouse anti-p53 (Pab 1801; 1:100; Santa Cruz Biotechnology), mouse anti-Bax (B-9; 1:100; Santa Cruz Biotechnology), mouse anti–phospho-stress-activated protein kinase/c-Jun N-terminal kinase (JNK) (Thr183/Tyr185) (no. 9255, clone G9; 1:1000; Cell Signaling Technology), mouse anti-TH (1:500; Calbiochem), rabbit anti-PINK1 (NB100-493; 1:500; Novus Biologicals, Littleton, CO), rabbit anti-DJ-1 (NB100-483; 1:500;

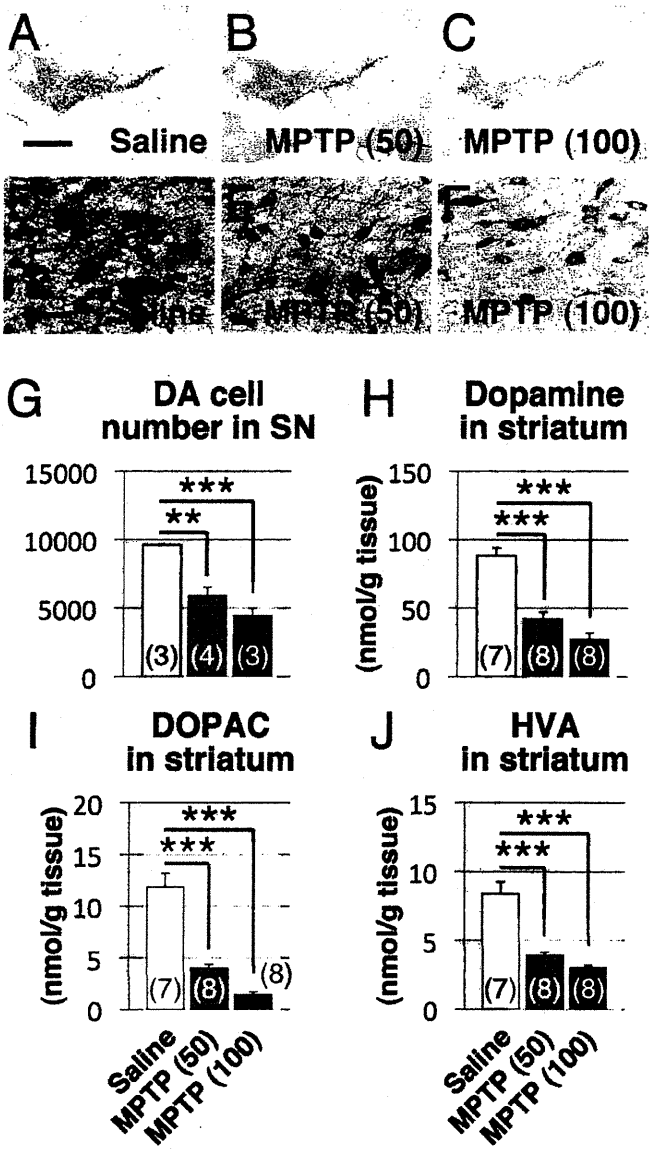

FIGURE 1. Long-term and high-dose MPTP models generated using Alzet osmotic minipumps. **(A–F)** Substantia nigra (SN) sections of saline- (Saline) and MPTP-minipump mice (50 mg/kg per day, MPTP [50] or 100 mg/kg per day MPTP [100]) immunostained for tyrosine hydroxylase (TH) and counterstained with Cresyl violet. **(G–J)** Numbers of dopaminergic (DA) cell bodies in the SN pars compacta **(G)**, and levels of dopamine **(H)**, 2-(3,4-dihydroxyphenyl)acetic acid (DOPAC) **(I)**, and homovanillic acid (HVA) in the striatum **(J)**. The implantation of MPTP-minipump caused a significant degeneration of the nigrostriatal DA neurons. Numbers of mice analyzed in each group are indicated within the bars. Data are mean ± SEM. **, $p < 0.01$; and ***, $p < 0.001$ (1-way analysis of variance followed by Tukey-Kramer post hoc test). Scale bars = **(A)** 500 μm (applicable to **A–C**); **(D)** 50 μm **(D–F)**.

Novus Biologicals), rabbit anti-Tom20 (FL-145; 1:200; Santa Cruz Biotechnology), rabbit anti-Ser129-phosphorylated αSyn (clone ab42906; 1:500; Abcam), mouse anti–Ser129-phosphorylated αSyn (clone pSyn#64; 1:1000; Wako Pure Chemical Industries, Ltd, Osaka, Japan), mouse anti-αSyn (clone 42; 1:500; BD Biosciences, Franklin Lakes, NJ), and mouse anti-actin antibodies (clone C4; 1:500; Millipore Corp).

Immunohistochemistry

Free-floating sections were washed in a PBS medium containing 0.05% Triton X-100 (PBS-T). When the rabbit and sheep primary antibodies were used, the sections were soaked with 10% Block Ace (Yukijirushi-Nyugyo Co, Sapporo, Japan) in PBS-T and then incubated with the primary antibodies dissolved in PBS-T containing 2% Block Ace at 4°C for 48 hours. When the mouse primary antibody was used, Vector M.O.M. Immunodetection Kit (Vector Laboratories, Inc, Burlingame, CA) was used for blocking and antibody dilution according to the instructions provided by the manufacturer. Subsequently, for fluorescent visualization of the antigens, the sections were incubated for 2 hours in fresh medium containing fluorescein isothiocyanate–conjugated anti-mouse or rabbit IgG and Cy3-conjugated anti-mouse, rabbit, or sheep IgG secondary antibodies (1:200–500; Jackson ImmunoResearch Laboratories, Inc, West Grove, PA). The sections were mounted on slide glass and coverslipped with Vectashield Mounting Medium with DAPI (Vector Laboratories). Images were captured using a confocal laser scanning microscope (LSM510; Zeiss, Jena, Germany). For colorimetric visualization of the antigen, the sections were incubated for 2 hours in fresh medium containing biotinylated

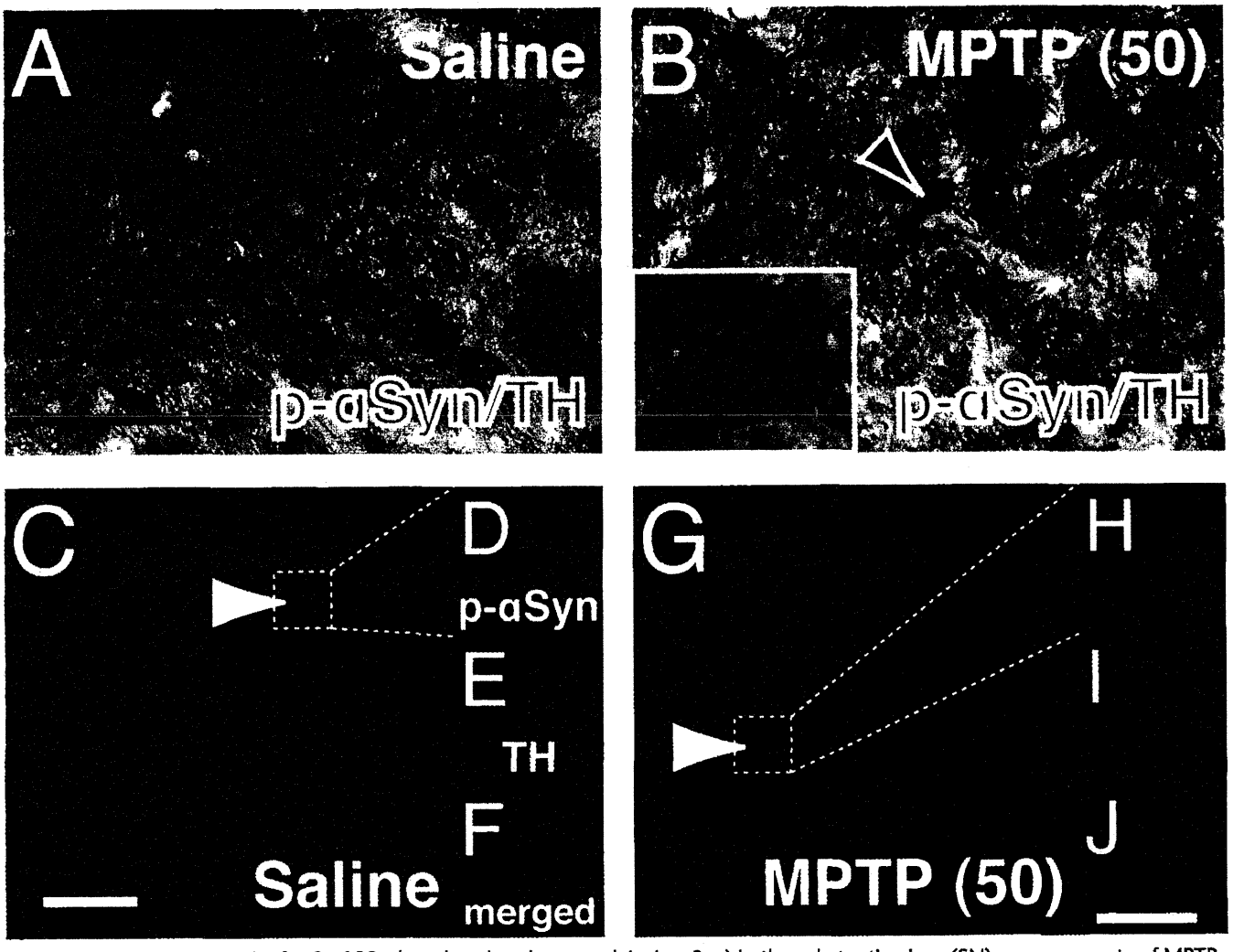

FIGURE 2. Immunoreactivity for Ser129-phosphorylated α-synuclein (p-αSyn) in the substantia nigra (SN) pars compacta of MPTP-minipump mice. **(A, B)** SN sections of saline- **(A)** or MPTP-minipump mice (50 mg/kg per day, MPTP [50]) **(B)** were coimmunostained for the p-αSyn (dark brown/purple) and tyrosine hydroxylase (TH) (brown). p-αSyn–positive cells (arrowhead, enlarged in **[B]** inset) were found in the SN of MPTP-minipump mice. **(C–J)** SN sections of saline- **(C–F)** and MPTP-minipump mice **(G–J)** coimmunostained for the p-αSyn **(C, D, F, G, H, J,** green) and TH **(C, E–G, I, J,** red), merged with anti–p-αSyn in **(C, F, G, J,** yellow) and visualized by fluorescence. Boxed areas in **(C)** and **(G)** are enlarged in **(D–F)** and **(H–J)**, respectively. Scale bars = **(A)** 50 μm (applicable to **B**); **(C)** 50 μm (applicable to **G**); **(J)** 10 μm (applicable to **D–F, H–J**).

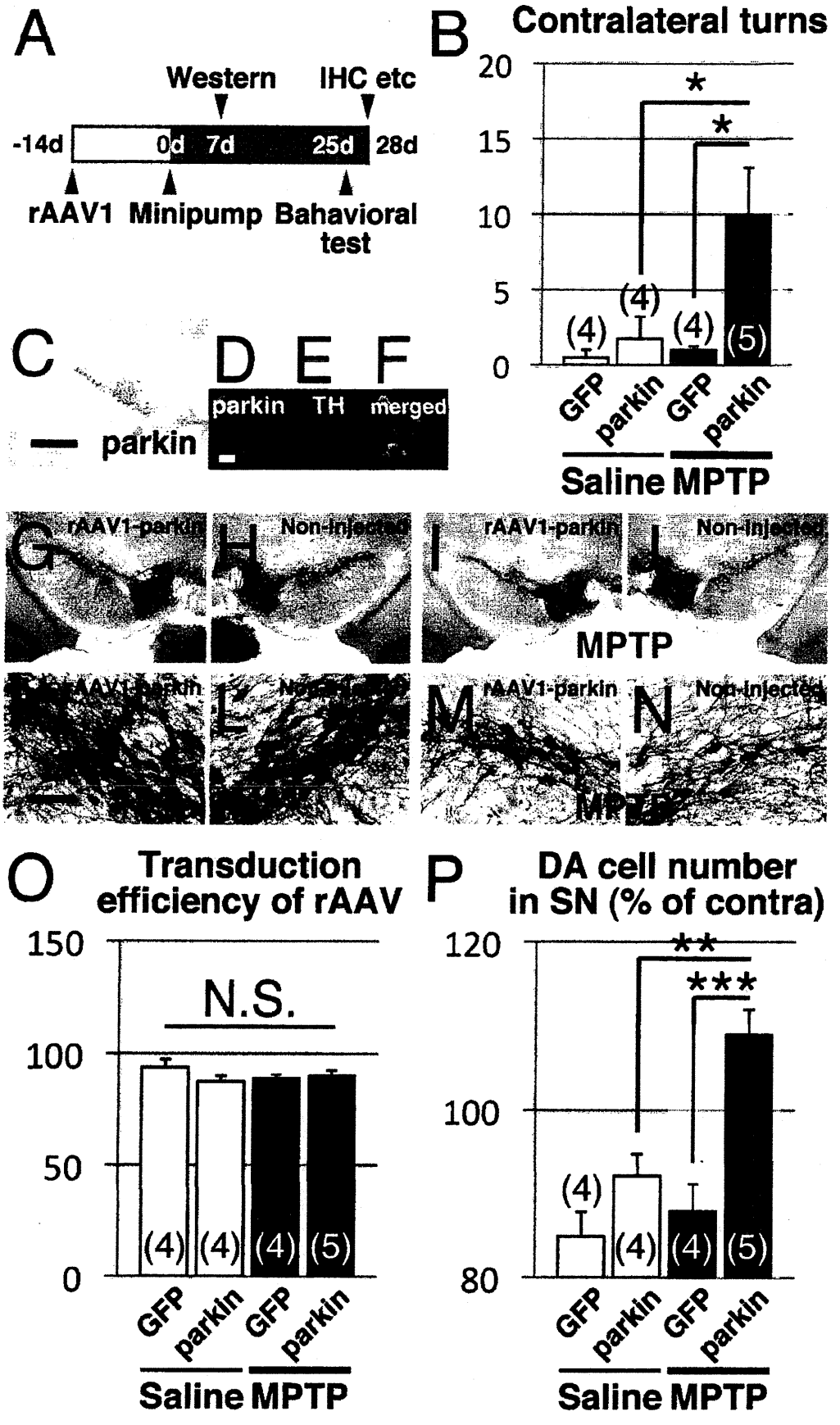

anti-mouse or rabbit IgG secondary antibody (1:500), followed by avidin-biotin-peroxidase complex (ABC Elite) (both from Vector Laboratories, Inc) for 1 hour. Then the sections were reacted in 0.05 mol/L Tris-HCl buffer (pH 7.6) containing 0.04% diaminobenzidine and 0.002% H_2O_2 with (dark brown/purple color) or without (brown color) 0.04% nickel chloride. Images were captured using a light microscope (ACT-1; Nikon Corp, Tokyo, Japan).

Western Blotting

Ventral midbrain tissues were sonicated in chilled CelLytic-MT mammalian tissue lysis/extraction reagent (Sigma) mixed with protease inhibitor cocktail set I (Calbiochem) and phosphatase inhibitor cocktail set V (Calbiochem). The protein concentration in the lysate was determined using BCA protein assay kit (Pierce, Rockford, IL). Each protein sample (10 μg) was resolved by SDS-PAGE by means of Compact-PAGE-twin (ATTO Corp, Tokyo, Japan) and then electrotransferred to Clear Blot Membrane-P (ATTO Corp) using powered BLOTmini (ATTO Corp). The membrane was washed in PBS, incubated for 1 hour in a PBS medium containing 50% ChemiBLOCKER (Millipore Corp) and 0.05% Tween-20, and then incubated for 24 hours with primary antibody in the same fresh medium. Subsequently, the membrane was incubated for 2 hours in fresh medium containing horseradish peroxidase–linked anti-mouse or rabbit IgG secondary antibody (1:10000; GE Healthcare Bio-Sciences, Uppsala, Sweden), followed by development of chemiluminescence using Amersham ECL Plus Western Blotting Detection System (GE Healthcare Bio-Sciences). The image was captured using LAS-3000 (Fujifilm, Tokyo, Japan) and quantified by Image Gauge software. Samples that showed intense protein expression of hrGFP or parkin were used for the subsequent investigations (Table).

Cell Counts

Every eighth 20-μm-thick serial section of the brain was immunostained for parkin (for mice injected with rAAV1-parkin) (Figure, Supplemental Digital Content 1, parts C–J, http://links.lww.com/NEN/A252) or hrGFP (for mice injected with rAAV1-hrGFP). Coimmunostaining for parkin or hrGFP and TH was also performed (Figure, Supplemental Digital Content 1, parts K-M, http://links.lww.com/NEN/A252). Mice that exhibited foreign protein expression in most DA cells in more than ~80% of the area of the entire rostrocaudal region of the SNpc were used for the subsequent investigations (Table). The rostrocaudal area of the SNpc immunopositive for foreign protein was determined in each mouse and used for DA cell counting and phosphorylated αSyn (p-αSyn)–positive cell counting. In every fourth serial section, the numbers of TH- and Nissl-double-positive cells in the SNpc were counted both in the rAAV1-injected and noninjected sides using a stereological method and in a blind manner, as previously reported (35, 38). In brief, SNpc cells with nuclei optimally visible by TH immunostaining and with nuclei, cytoplasm, and nucleoli prominently stained by Nissl staining were counted. To avoid

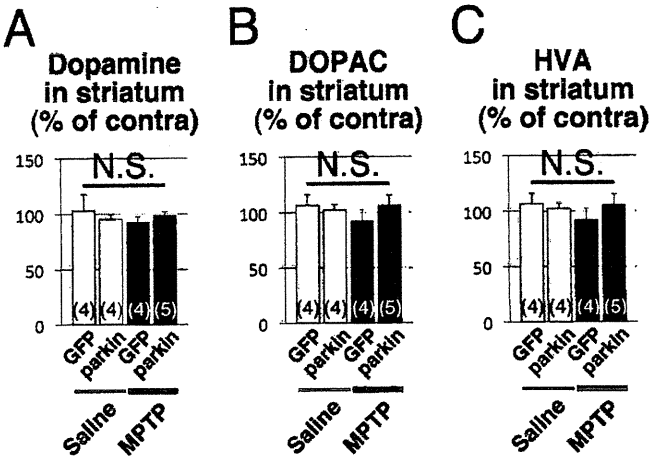

FIGURE 4. Effect of recombinant adeno-associated viral (rAAV1) vector-parkin delivery on striatal levels of dopamine and its metabolites. **(A–C)** The striatal levels of dopamine **(A)**, 2-(3,4-dihydroxyphenyl)acetic acid (DOPAC) **(B)**, and homovanillic acid (HVA) **(C)** in rAAV1-humanized recombinant green fluorescent protein (hrGFP)–injected (denoted as GFP) and the rAAV1-parkin–injected (parkin) saline- (Saline) and MPTP-minipump mice (MPTP). There were no effects on amounts of these compounds. Numbers of analyzed mice in each group are indicated within the bars. Data are expressed as percentage of the contralateral side (% of contra). N.S., not significant (1-way analysis of variance).

FIGURE 3. Recombinant adeno-associated viral (rAAV1) vector-parkin–mediated prevention of behavioral deficit and dopaminergic (DA) cell loss in MPTP-minipump mice. **(A)** Time schedule for gene delivery experiment with rAAV1-parkin. At day 14 after intranigral injection of rAAV1 vector, Alzet osmotic minipumps were implanted i.p. to deliver saline or MPTP at a dose of 50 mg/kg per day for 7 (Western blotting) or 28 days (immunohistochemistry and dopamine measurement). Apomorphine-induced behavioral change was analyzed at day 25 after implantation. **(B)** Apomorphine-induced contralateral turns were counted in rAAV1-humanized recombinant green fluorescent protein (hrGFP)-injected (GFP) or rAAV1-parkin–injected (parkin) saline- (Saline) or MPTP-minipump mice. There was a significant increase in the number of contralateral turns in rAAV1-parkin/MPTP mice. **(C–F)** Substantia nigra (SN) sections of rAAV1-parkin/MPTP mice immunostained for parkin (**C**, brown, **D**, green), and tyrosine hydroxylase (TH) (**E**, red, merged with anti-parkin in **F**, yellow). **(G–N)** Representative photomicrographs of TH- and Nissl-double-positive cells in the ipsilateral (rAAV1-parkin, **G, I, K, M**), and contralateral (noninjected) sides of the SN pars compacta **(H, J, L, N)**, in saline- **(G, H, K, L)** or MPTP-minipump mice **(I, J, M, N)**. **(O)** Transduction efficiencies of the rAAV1 vectors, expressed as percent of the entire rostrocaudal region of the SN. There were no significant differences among the groups. **(P)** Counts of DA cell bodies in the SNpc. Data are expressed as percentage of the contralateral side (% of contra); that is, the cell number in the rAAV1-injected side over that in the noninjected side. rAAV1-parkin ameliorated MPTP-induced DA cell loss. Numbers of mice in each group are indicated within the bars. Data are mean ± SEM. *, $p < 0.05$; **, $p < 0.01$; ***, $p < 0.001$; and N.S., not significant (1-way analysis of variance followed by Tukey-Kramer post hoc test). Scale bars = **(C)** 500 μm (applicable to **G–J**); **(D)** 10 μm (applicable to **D–F**); **(K)** 50 μm (applicable to **K–N**).

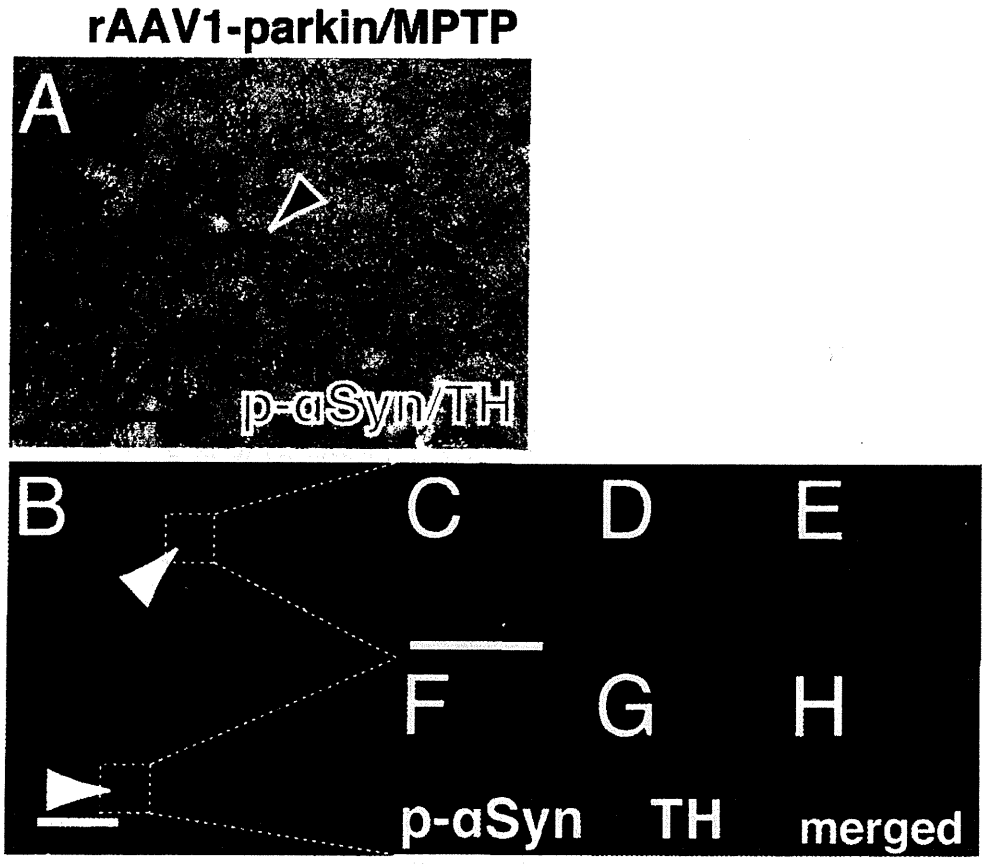

I

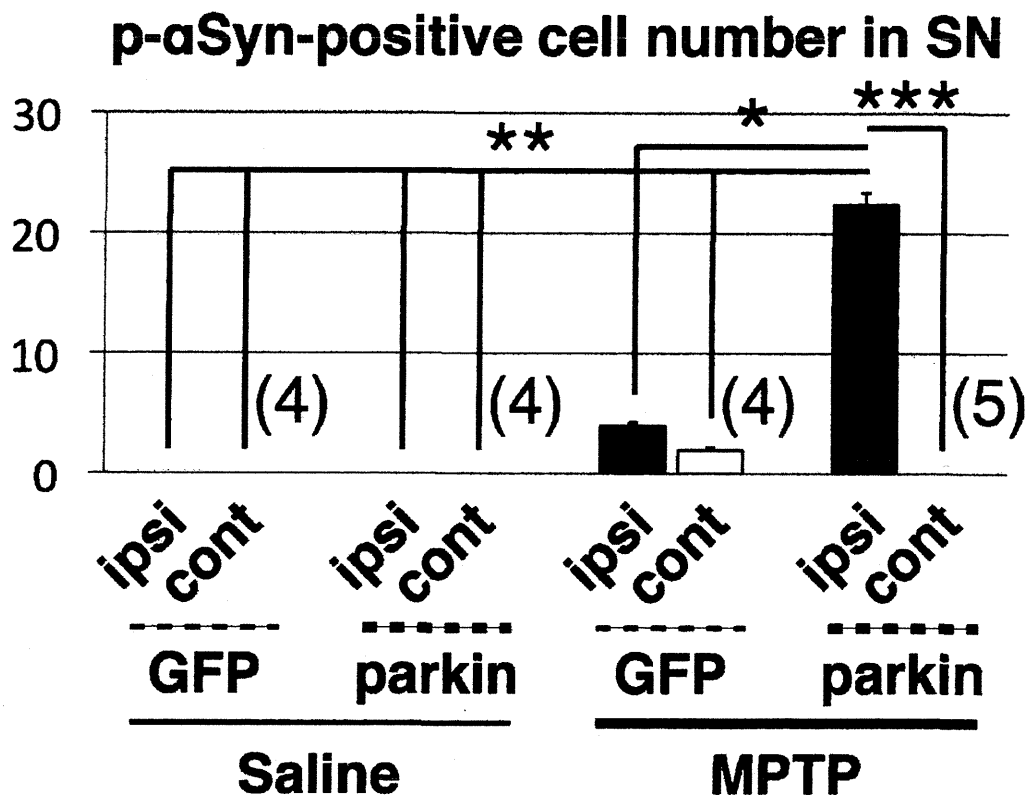

double counting of neurons with unusual shapes, TH- and Nissl-double-positive cells were counted only when their nuclei and nucleoli were optimally visualized. Data were expressed as percentage of the contralateral side, that is, the cell number in the rAAV1-injected side over that in the noninjected side. The numbers of the p-αSyn–positive cells visualized by diaminobenzidine with nickel chloride were counted in every eighth serial section of the SN.

Determination of the Striatal Levels of Dopamine and its Metabolites by High-Performance Liquid Chromatography

Frozen striatal tissues were sonicated in chilled 0.1 mol/L perchloric acid. The samples were centrifuged (20,000 × *g* for 10 minutes at 4°C), and the resulting supernatants were used for the measurement of dopamine, 2-(3,4-dihydroxyphenyl)-acetic acid (DOPAC), and homovanillic acid (HVA) concentrations. The high-performance liquid chromatography (HPLC) system equipped with an 8-electrode coulometric electrochemical detection system (ESA-400; ESA, Inc, Chelmsford, MA) and a reverse-phase C18 column (150 × 4.6 mm; ODS-100s; Tosoh, Tokyo, Japan) was used. The concentrations of dopamine, DOPAC, and HVA were determined in nanomoles per gram of tissue.

Determination of the Striatal Level of 1-Methyl-4-Phenylpyridinium (MPP^+) by HPLC

Mice were killed 24 hours after minipump implantation. Striatal tissues were sonicated in chilled 0.1 mol/L perchloric acid containing 0.1 mmol/L EDTA and an internal standard, 10 mmol/L 4-phenylpyridine (Sigma-Aldrich Corp). The samples were centrifuged (20,000 × *g* for 10 minutes at 4°C), and the resulting supernatants were used for MPP^+ concentration measurement (nmol/g of tissue). The HPLC system AKTA explorer (GE Healthcare Bio-Sciences) equipped with a reverse-phase C18 column (150 × 4.6 mm; ODS-100s; Tosoh) was used.

Statistical Analysis

All data are expressed as mean ± SEM. Two-tailed Student *t*-test (for 2 groups) and 1-way analysis of variance (ANOVA), followed by Tukey-Kramer post hoc test (for ≥3 groups) were applied. A p value less than 0.05 denoted statistically significant differences.

RESULTS

Generation of a High-Dose and Long-Term MPTP Infusion Model Using Alzet Osmotic Minipumps

The 50- and 100-mg/kg-per-day MPTP-minipump mice had 61.3% ± 6.3% ($p = 0.003262$; $df = 9$; 1-way ANOVA followed by Tukey-Kramer post hoc test) and 46.1% ± 5.6% ($p = 0.0006822$) of DA cell bodies in the SNpc found in the saline controls (Figs. 1A–G); they had 48.1% ± 5.1% ($p = 6.646 \times 10^{-6}$; $df = 22$) and 31.2% ± 5.1% ($p = 9.808 \times 10^{-8}$) of dopamine in the striatum found in the saline group, respectively (Fig. 1H). Dopamine metabolites, DOPAC and HVA, were also decreased (Figs. 1I, J). Levels of striatal MPP^+ (the active metabolite of MPTP) were 4.23 ± 1.46 nmol/g tissue ($p < 0.05$ vs the saline control group) and 7.05 ± 0.64 nmol/g tissue ($p < 0.001$ vs control) for the 50- and 100-mg/kg-per-day regimens, respectively ($p < 0.05$ and $p < 0.001$, by 1-way ANOVA followed by Tukey-Kramer post hoc test). Despite the loss of nigrostriatal DA neurons 28 days after the implantation, behavioral changes were not evident by rotarod test (even in the 100-mg/kg-per-day MPTP group) at 25 days after implantation of minipumps (latency time to fall: 198.3 ± 26.0 seconds in the saline group and 229.7 ± 17.2 seconds in the 100-mg/kg-per-day MPTP group; $p = 0.3461$).

Immunoreactivity for the Ser129-Phosphorylated αSyn in the SN of MPTP-Minipump Mice

Fornai et al (39) previously observed electron-dense and fibrillar neuronal inclusions containing αSyn in the SN of MPTP-minipump model mice. One of the critical pathogenic modifications of αSyn is the phosphorylation at Ser129 residue (40); therefore, we examined Ser129-p-αSyn immunoreactivity in the SN of our MPTP-minipump mice. In preliminary studies, the anti-p-αSyn antibody was evaluated using nigral sections of mice that had received a stereotaxic intranigral injection of rAAV1 vector encoding human αSyn (Figure, Supplemental Digital Content 2, http://links.lww.com/NEN/A253). The antibody reacted specifically with DA cell bodies in the ipsilateral side of the SN (Figure, Supplemental Digital Content 2, parts B-E, I-K, http://links.lww.com/NEN/A253) in which human αSyn is overexpressed (Figure, Supplemental Digital Content 2, parts 2 A, D, J, http://links.lww.com/NEN/A253). We found a small number of p-αSyn–immunopositive cells in the SN of MPTP-minipump (50 mg/kg per day) mice (Figs. 2B, G–J; see also Fig. 5I). These cells were not seen in saline-minipump mice (Figs. 2A, C–F; also see Fig. 5I).

Amelioration of Nigral DA Cell Loss by rAAV1-Mediated Parkin Overexpression in MPTP-Minipump Mice

We next investigated the effect of rAAV1-mediated overexpression of parkin on the survival of DA neurons in MPTP-minipump mice. High-titer rAAV1-parkin or rAAV1-hrGFP was injected unilaterally into the SN of C57BL/6 mice.

FIGURE 5. Ser129-phosphorylated αSyn (p-αSyn) immunoreactivity in the substantia nigra (SN) pars compacta of MPTP-minipump mice injected with recombinant adeno-associated viral (rAAV1) vector-parkin. **(A)** SN sections of rAAV1-parkin/MPTP mice coimmunostained for the p-αSyn (dark brown/purple) and tyrosine hydroxylase (TH) (brown) and visualized using diaminobenzidine. A p-αSyn–positive cell is indicated by arrowhead. **(B–H)** SN sections of rAAV1-parkin/MPTP mice coimmunostained for p-αSyn (**B, C, E, F, H**, green) and TH (**B, D, E, G, H**, red), merged with anti-p-αSyn (**B, E, H**, yellow), and visualized by fluorescence. Boxed areas in **(B)** are enlarged in (**C–E** and **F–H**). **(I)** Counts of p-αSyn–positive cells in the SN, visualized by diaminobenzidine. Injection of rAAV1-parkin significantly increased the p-αSyn–positive cells in MPTP-minipump mice. Numbers of analyzed mice in each group are indicated. Data are mean ± SEM. *, $p < 0.05$; **, $p < 0.01$; and ***, $p < 0.001$ (1-way analysis of variance followed by Tukey-Kramer post hoc test). Scale bars = **(A)** 50 μm; **(B)** 50 μm; **(C)** 10 μm (applicable to **(C–H)**).